Water Dynamics About Selected Monosaccharides in Solution

Dissertation presented to the

University of Cape Town

in fulfillment of the requirements for the degree of

Master of Science

By

Allistair F. Mokoena
BSc Hons
Supervisors: Prof. Kevin J. Naidoo
Dr. Gerhard A. Venter

Department of Chemistry
University of Cape Town
2014

Acknowledgements

I am thankful to the University of Cape Town and the South African Nuclear Human Asset and Research Programme for financial aid.

I also thank members of the Scientific Computing Research Unit for all the insightful discussions and the valuable contributions that lead to the completion of this work. A special thanks to Louise Bezuidenhout for her endless support.

To my friends and family, I am grateful for the many ways in which they showed their support. To my mother, thank you for being there when I needed you the most.

It has been a long journey, but one that has been filled with intriguing research aspects and it was made possible through the guidance of my supervisors, Prof. Kevin J. Naidoo and Dr. Gerhard A. Venter. I am grateful for their assistance throughout the project.

Dedicated to my late grandparents (Ramokone & Malesela Manamela). It would have never been possible without them.

Plagiarism declaration

1. I know that plagiarism is wrong. Plagiarism is to use another's work and pretend that it is one's own.

2. Each contribution to, and quotation in, this dissertation from the work(s) of other people has been attributed, and has been cited and referenced.

3. This dissertation is my own work.

4. I have not allowed, and will not allow, anyone to copy my work with the intention of passing it off as his or her own work.

5. I acknowledge that copying someone else's work, or part of it, is wrong, and declare that this is my own work.

Signature:_____

Abstract

The solubility of molecules in water is governed, amongst other things, by the inherent properties of the solute molecules and water molecules. Water molecules are able to simultaneously form hydrogen bonds as donors and acceptors and thus have unique properties as solvent molecules. These properties influence how water interacts with solute molecules. The mechanism of hydrogen bond exchange plays a role in the hydration of solute molecules. A key to understanding some of the biological processes lies in understanding how solutes interact with water.

In this thesis, the hydration of monosaccharides has been studied using computational methods. The hydration structure is elucidated by pair distribution functions and spatial distribution functions. Hydrogen bond exchange dynamics were investigated on the basis of the molecular jump mechanism.

Evaluation of the hydrogen bond exchange dynamics reveals two possible pathways. The first pathway corresponds to the molecular jump mechanism reported in literature. The second pathway is described. This pathway provides details on the water-hydroxyl interactions taking place around the monosaccharides. It is shown that the presence of a primary alcohol on pyranose based molecules induces a configuration that allows favourable interactions between water molecules and hydroxyl groups on the sugar molecules. A region of high water density is formed between the primary alcohol, ring oxygen and the hydroxyl on the anomeric carbon. This is due to rotations by water molecules from one hydroxyl, to the adjacent hydroxyl on the sugar molecule. It is not only the presence of the primary alcohol that plays a role in the hydration of the monosaccharides. The relative position of the hydroxyl on the anomeric carbon is shown to create a topology conducive of

hydroxyl to hydroxyl hydrogen bond exchanges. The hydration of monosaccharides is rationalised by these effects.

Table of Contents

List of Figures

Chapter 1

Chapter 2

Chapter 3

Chapter 4

List of Tables

Chapter 2

Chapter 4

Chapter 1 The relationship between saccharide and water in solution

1.1 Carbohydrates

Carbohydrates are organic molecules containing carbon, hydrogen and oxygen as their basic elements. Other elements such as nitrogen, sulphur and phosphorus can form part of a carbohydrate molecule. Carbohydrates form part of most life-sustaining processes in living organisms[1] and as such, have been the subject of many studies in the scientific community.[1a-c, 2]

Carbohydrates in their simplest form occur as monosaccharides. These can exist in an open-chain form or in a closed ring form. Glucose, for example, in its open-chain form can cyclize to form a hemiacetal (Figure 1.1) which is the more favoured form in solution.[3]

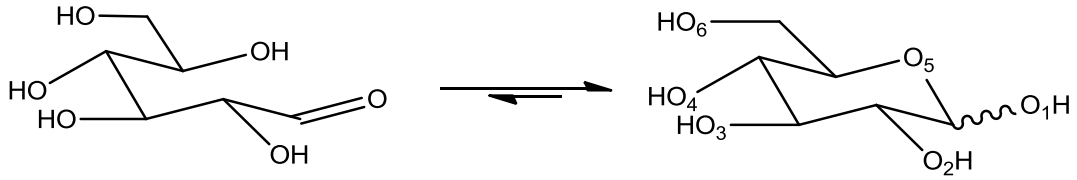

Figure 1.1: Interconvertion of glucose from the open chain structure (left) to a six-membered ring structure (right).

The ring form exists mainly in the $^4C_1$ chair conformation and has two anomeric forms, α and β, the latter has been shown to be the most abundant in aqueous solution.[4] However, the α-anomer is believed to be more stable in the gas phase, due to the anomeric effect.[5] The argument for the β-anomer abundance in solution, is its ability to fit in the trymidite ice lattice where the water-water hydrogen bonds are replaced by the water-glucose hydrogen bonds.[6] It is also argued that the gas phase preference for the α-anomer is due to basis set dependence in *ab anitio*

studies. The α/β energy differences are said to decrease with increasing quality of the calculation.[7]

1.1.1 Monosaccharide conformations

The conformational flexibility of a polysaccharide (a chain of monosaccharides) can be attributed to properties of the monosaccharides. A polysaccharide is formed by linked monosaccharides. These linkages termed glycosidic linkages, are formed when hydroxyl groups on two monosaccharides undergo a condensation reaction. The linkages are referred to as alpha or beta depending on their relative orientation to the C1 carbon. The hydroxyl groups can either be primary (attached to the methyl carbon) or secondary (attached to a carbon atom on the ring). Due to the number of hydroxyls available on the monosaccharides, there exist numerous possible linkages. Three of the common linkages are illustrated in Figure 1.2.

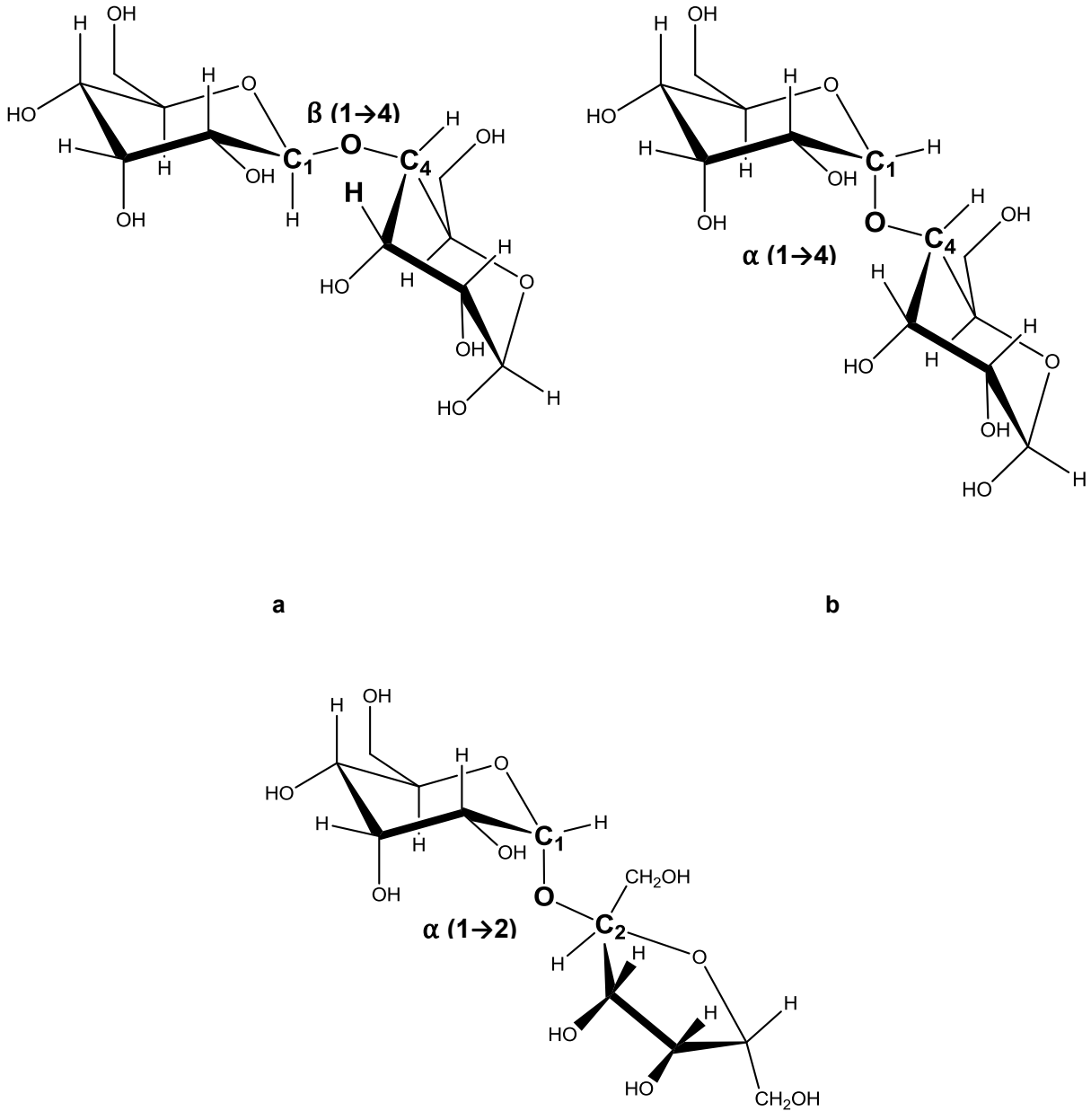

Figure 1.2: Glycosidic linkages formed in (a) cellobiose (b) maltose, and (c) sucrose.

When a linkage involves the primary alcohol, there is added degrees of rotational freedom and this provides further flexibility to the polysaccharide. There are three configurations the primary alcohol can have, gauche-gauche (gg), gauche-trans (gt) and trans-gauche (tg). The first letter refers to the O5 – C5 – C6 – O6 dihedral while the second refers to the C4 – C5 – C6 – O6 dihedral. An illustration of the different configurations is given in Figure 1.3

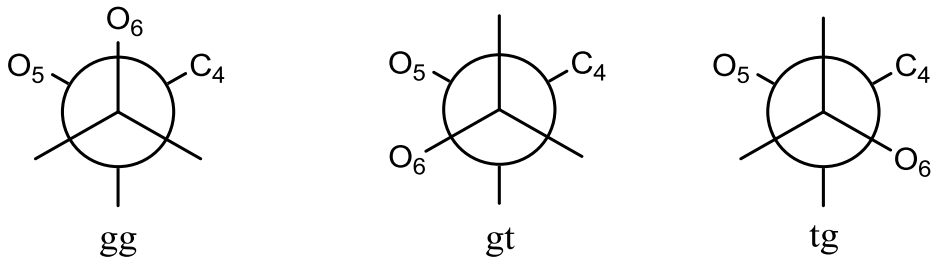

Figure 1.3: Primary alcohol rotamers of a pyranose ring.

The conformations of the monosaccharides in their closed ring form allow for the hydroxyl groups to form intramolecular hydrogen bonds. In vacuum there can be at least two intramolecular hydrogen bonds present in glucose. It has been show that in vacuum, the conformational preference in β-D-glucopyranose is gg>tg>gt and this changes to gt>gg>tg in solution. This change has been attributed to the intramolecular hydrogen bond that forms between O4 and O6.[2c]

The six-membered pyranose rings are known to exist in various pucker conformations.[8] A total of 38 ring conformations exist, of these, the basic conformations include six boat (B), six skew-boat (S), twelve half-chair (H), twelve envelopes (E) and two chair (C) conformers. [9] The boat, skew-boat, half-chair and chair conformation have four atoms lying in one plane while the envelope has five atoms in a plane. This is depicted in Figure 1.4

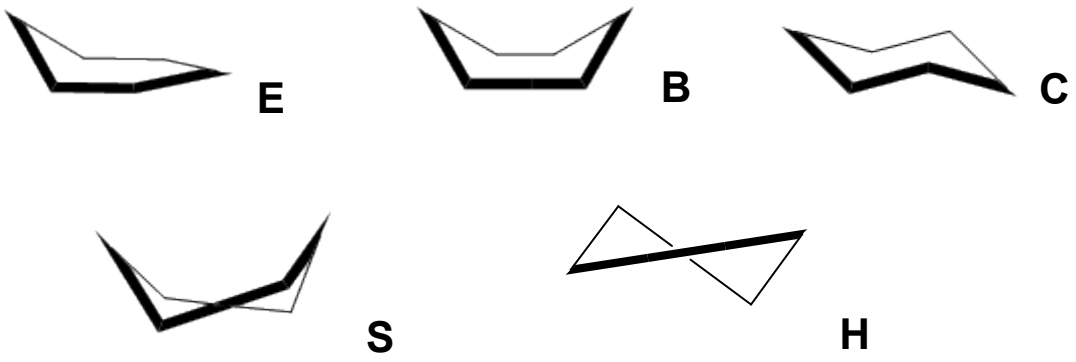

Figure 1.4: Five conformers of six-membered rings.

The interconversion between the conformer can be illustrated using a well-known diagram, Stoddart's diagram in Figure 1.5

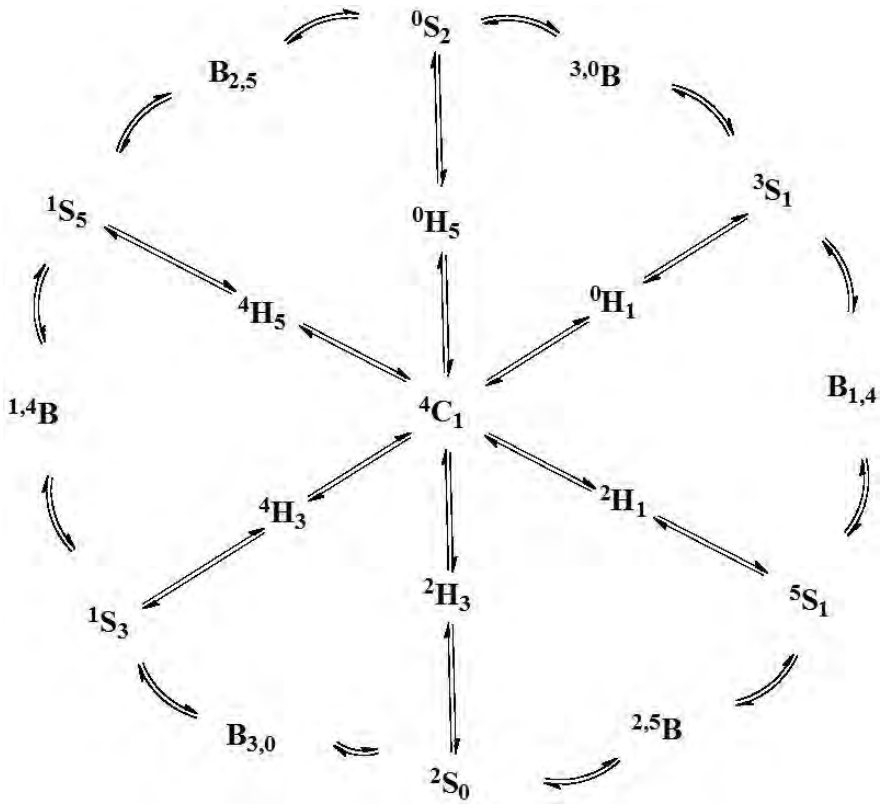

Figure 1.5: The relationship between the pucker conformations of pyranose rings. Reproduced from ref [9].

1.1.2 Carbohydrate-water interactions

The structuring of water around solutes plays an important role in their reactivity.[10] The presence of a solute perturbs the hydrogen bond network. Depending on the nature of the solute, water molecules arrange themselves in a particular manner around the solute.[11] Techniques such as depolarized Rayleigh scattering, quasielastic neutron scattering,[12] and terahertz absorption spectroscopy[13] experiments have been employed to study the structure and dynamics of water molecules around biomolecules.[10] In these experiments it was found that the water molecules proximal to the sugar molecule lose their tetrahedral arrangement and a new water structure is imposed by the sugar molecule. Near infrared spectroscopy has also been used to study water-sugar interactions.[14] In the study, water-sugar interactions were studied and interpreted in terms of the variations induced in the water structure with reference to that of pure water. A solute can either be a *structure-breaker* or *structure-maker*, i.e. a structure-breaker perturbs the structure of liquid water and a structure-maker reinforces the structure. It has been shown that glucose, fructose and sucrose are structure-breakers at low concentrations and structure-makers at high concentrations.[14]

It has been suggested that the presence of a hydroxyl group alone is not enough to improve the solute-water interactions in organic compounds.[15] A recent study on hydration numbers of cyclic molecules revealed that the conformational flexibility of the molecules corresponds with their hydration number.[16] It was shown that for more rigid pyranose based molecules, the ring puckering frequency is lower compared to the cyclohexane based molecules and thus enhances the water-solute interactions.

Theoretical studies of the water structure around α-D-glucopyranose have shown that hydroxyl groups on sugars impose a tetrahedral-like ordering on water molecules interacting with them, similar to the tetrahedral arrangement of the local structure of water.[17] It was also suggested that the most favorable hydration of a sugar is achieved when the hydration of each hydroxyl group is such that it perturbs its neighbours' water molecules the least. It has also been shown that translational mobility of water molecules around carbohydrates is slowed down.[18],[19] Wang et al. performed a study on the behavior of interfacial water molecules around α-maltose and found that there is no general trend in the diffusion coefficient of water around the different atoms types in the sugar.[18] Molecular dynamics simulations have shown that many important dynamical properties of water in the hydration shells of important biological compounds are in the picosecond and subpicosecond time scales.[20]

Elucidating the dynamics of water around carbohydrates would help in developing a general understanding on how the carbohydrate structure and topology affects the molecule's interaction with water. Glucose and xylose molecules serve as good models for studying carbohydrate-water interactions because of their small structure. They contain only three different atom types and their functional groups are also found on proteins and nucleic acids.

1.1.3 Intra and intermolecular competition in monosaccharide hydration

1.1.3.1 Hydrogen bonding

Water molecules have the ability to simultaneously make hydrogen bonds both as acceptors and donors.[17, 21] The result is that water has a highly ordered and directional arrangement in the aqueous condensed phase.[22] A hydrogen bond network is formed when a water molecule's hydrogen atoms are directed towards the neighbouring molecule's oxygen lone pairs and its lone pairs are directed towards hydrogen atoms of other neighboring water molecules. The lone pairs and hydrogen atoms lie at the vertices of a tetrahedron. This tetrahedral structure is also observed in ice. Many of water's properties are attributed to this network. The exact connectivity of the hydrogen bond network constantly changes. An illustration of the network is depicted in Figure 1.6.

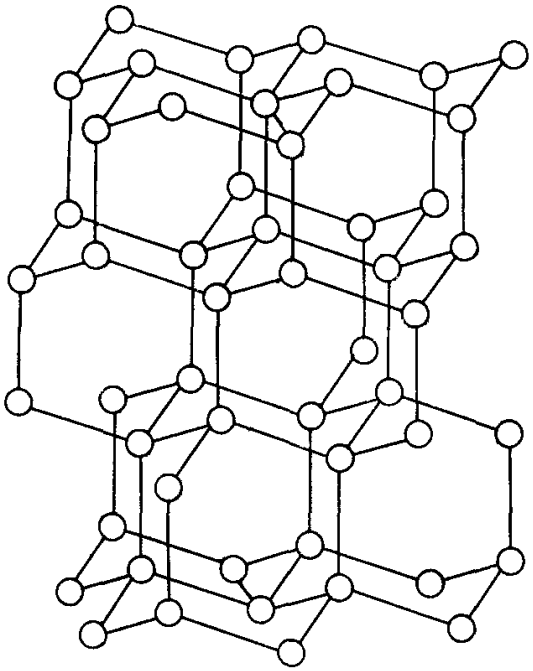

Figure 1.6: Structure of hexagonal ice (Ih) represented by the oxygen backbone as depicted in ref [22].

The definition of an hydrogen bond is essentially arbitrary and thus there are various definitions.[23] Some of these are better suited for certain experimental techniques.[24]

Geometric, energetic and definitions involving orbital occupancy have been used to study the local structure of water.[23] In this work the geometric definition has been used. The criteria used in identifying hydrogen bonds are as follows:

- $R_{O\text{-}O} < 3.4$ Å
- $R_{O\text{-}H} < 2.45$ Å
- $\Theta_{O\text{-}H\cdots O} > 120°$

The angle criterion was relaxed to allow for detection of intramolecular hydrogen bonds in the monosaccharides.

1.1.3.2 Hydration of simple carbohydrates

It was shown through theoretical studies that intramolecular hydrogen bonds are formed between hydroxyls on glucose. The existence of such hydrogen bonds is observed mainly in simulations performed in vacuum. In the α-anomer, the $^1C_4$ conformation is favoured over the $^4C_1$. Hydration of glucose is said to affect the purkered conformations of the molecule as it allows for lower energy costs for transition between the chair conformations compared to transitions in vaccum.[4b] However, in the β-anomer solvation effects are not as significant for conformational transitions.

Intramolecular hydrogen bonds have been shown to form not only in monosaccharides but also in disaccharides.[25] These intramolecular hydrogen bonds are supplanted by intermolecular hydrogen bonds in solution, this despite a previous study that showed that the strengths of intramolecular and intermolecular hydrogen bonds in carbohydrates are similar. [26] This deficiency in intramolecular hydrogen bonds is due to the positional constraints of the hydroxyls imposed by the geometry

of the sugar molecule. The most populated intramolecular hydrogen bond is that of the primary alcohol and O_4 hydroxyl in glucose. This hydrogen bond has been shown to contribute significantly to the primary alcohol conformation. [2c]

Studies have shown that sugars retard the motion of water molecules in their hydration shells. A number of experimental techniques; extended dielectric depolarized light scattering (EDLS),[27] depolarized Rayleigh scattering (DRS), [10] infrared spectroscopy (IR),[28] NMR,[29] and broadband dielectric spectroscopy (BDS)[30] have reported a varying range of the slow down rates (1.7 – 3.3) induced by sugars.

1.1.4 Carbohydrate-metal interactions

Metal-carbohydrate interactions play an important role in many systems. The structural properties brought about through complexation of metals to carbohydrates can be used in selective metal ion sensors.[31],[32] It has been reported that mannose-binding protein cannot perform its function without the Ca^{2+}-carbohydrate interaction.[33] Theoretical studies conducted on the binding of metal ions of simple carbohydrates showed that metal ions have preferential binding sites on the carbohydrate. This is due to the limited motion of the hydroxyl groups on the carbohydrate and hence they cannot compete with the solvent molecules for binding to the metal ion.[34] The study showed that there are mainly two favorable binding sites on *cis*-inositol, i.e. axial-axial-axial (ax-ax-ax), defined by three hydroxyl groups in the axial position and axial-equatorial-axial (ax-eq-ax) where one of the hydroxyls are in the equatorial position and the other two axial. Figure 1.7 illustrates the binding sites on cis-inositol.

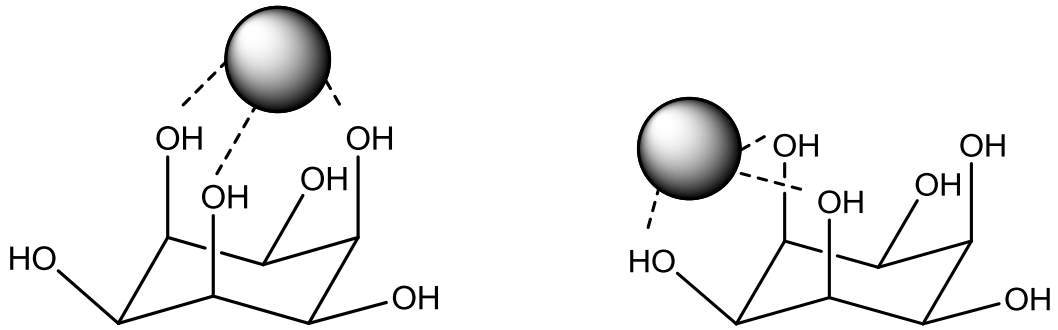

Figure 1.7: Preferred binding sites on *cis*-inositol. (a) ax-ax-ax. (b) ax-eq-ax. Taken from ref [34]

For β-D-glucopyranose a metal ion binds to two hydroxyls and when the primary alcohol is in the proximity of the binding site the number can go up to three.[34]

1.1.5 Objectives

The aim of this study is to investigate the dynamics of water around selected monosaccharides. The objective is to discover the relationship between the primary alcohol, the ring oxygen and the secondary alcohol on the anomeric carbon of the sugars, as it affects monosaccharide water interactions and solubility. To achieve this, the methods commonly used in computer simulations of monosaccharides are reviewed in Chapter 2. The choice of techniques used in this thesis will be discussed therein. This is followed by investigating a water reorientation mechanism recently discovered by Laage[35] in Chapter 3. Analysis of the water-sugar interactions is performed in Chapter 4. This entails determining the water structure around each monosaccharide. This is followed by calculating the dynamical properties of water in the hydration spheres. These include translational diffusion, rotational diffusion and the mechanism of water reorientation in the hydration shells. Solute properties such as diffusion will also be studied.

All these dynamical properties will be studied for β-D-glucopyranose, α-D-glucopyranose, β-D-xylopyranose and α-D-xylopyranose to establish the effect of the solute on its surrounding water molecules and how the individual properties contribute to the overall behavior of each monosaccharide in solution. The molecules to be studied are shown in Figure 1.8.

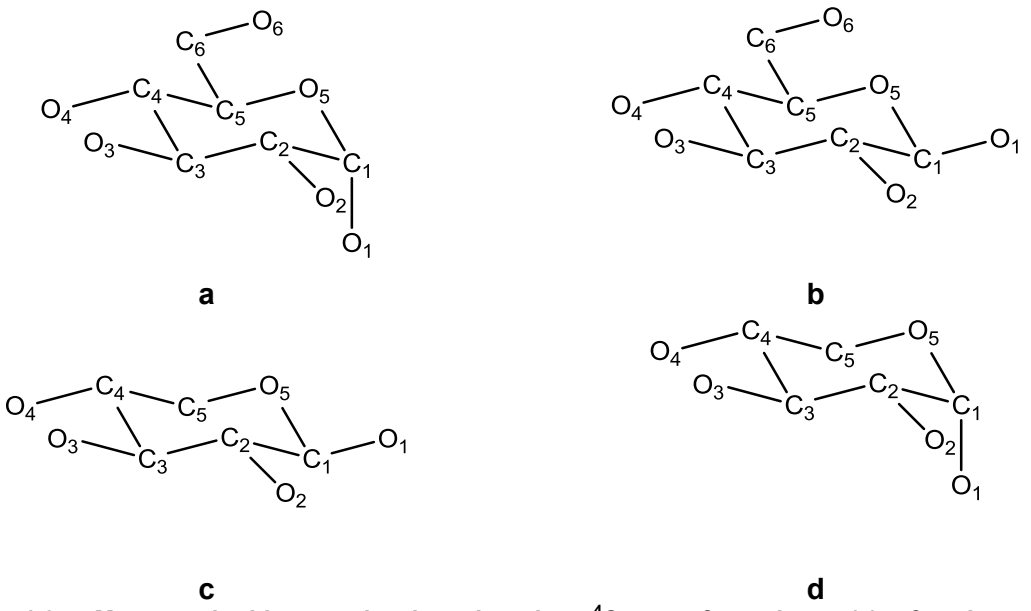

Figure 1.8: Monosaccharides molecules in the $^4C_1$ conformation. (a) β-D-glucopyranose (b) α-D-glucopyranose (c) β-D-xylopyranose (d) α-D-xylopyranose. Hydrogen atoms are omitted. This numbering scheme is used in subsequent chapters.

A summary of the findings will be presented in the concluding chapter.

Chapter 2 Computational Methods

2.1 Molecular Mechanics

2.1.1 Empirical Force Fields

Investigating molecular properties is one of a chemist's main objectives. For properties that cannot be accurately studied by experimental methods molecular modelling is an alternative and complementary method of studying molecular properties. Molecular modelling can be divided into two main categories, which is Quantum Mechanics (QM) and Molecular Mechanics (MM). Quantum mechanical methods are based on the electrons in a system and as such calculations for large system require long computation times. In the case of molecular mechanics the energy of a system is calculated based on the atoms' nuclear positions and as a result large systems can be modelled in shorter time periods.[36] However, properties that depend on the electronic structure of molecules cannot be determined using molecular mechanics and although very accurate results can be obtained, this technique provides no information on the electronic properties of systems.

The Born-Oppenheimer approximation allows for calculation of the potential energy from nuclear positions only. It states that the motion of the electrons can be decoupled from the motion of the nuclei and the nuclear and electronic energy can be calculated independently.[37]

$$\psi_{tot}(nuclei, electrons) = \psi(nuclei)\psi(electrons) \quad \textbf{(2.1)}$$

The total internal energy of the system can be expressed as the sum of the nuclear and electronic energy. To calculate the total internal energy, only the electronic

Schrödinger equation needs to be solved and the internuclear repulsion term is then added.

The motion of the nuclei is stationary relative to that of the electrons and the nuclei see the electrons as a smeared-out cloud of negative charge. The electrons are in fixed relative positions around the nuclei. This cloud defines the surface of the molecule and gives rise to a molecule shape.

In molecular mechanics, molecules are represented as a collection of balls (atoms) held together by springs (bonds). This mechanical model is used to calculate the potential energy. The energy terms and parameters in them make up a *Force Field.* The negative of the first derivative of the potential energy of an atom with respect to displacement along a particular direction is the force on the atom and hence the term Force Field.[37] The parameters used in the force fields can be obtained from experiment and some are calculated from quantum mechanical methods. Force fields are thus also referred to as *empirical* force fields. The potential energy function describes how the energy of the system is related to the structure. The general functional form of a force field is given in equation (2.2):[38]

$$\Upsilon(r^N) = \sum_{bonds} \frac{K_i}{2}(l_i - l_{i,0})^2 + \sum_{angles} \frac{K_i}{2}(\theta_i - \theta_{i,0})^2 + \sum_{torsions} \frac{K_i}{2}(1 + \cos(n\omega - \gamma) + \sum_{\substack{impoper \\ dihedrals}} K\varphi(\varphi_i - \varphi_{i,0})^2 + \sum_{Urey-Bradley} K_{UB}(r_{1,3} - r_{1,3;0})^2$$
$$+ \sum_{i=1}^{N}\sum_{j=1}^{N}\left(4\varepsilon_{ij}\left[\left(\frac{\sigma_{ij}}{r_{ij}}\right)^{12} - \left(\frac{\sigma_{ij}}{r_{ij}}\right)^{6}\right] + \frac{q_i q_j}{4\pi\varepsilon_0 r_{ij}}\right)$$

(2.2)

$\Upsilon(r^N)$ represents the potential energy as a function of the positions of N particles. The intramolecular energy is described by the first five terms. The first term gives the interaction of bonded atoms and is modelled by a harmonic potential that measures

the increase in energy as a function of the change in the bond length, l_i, from the equilibrium bond length, $l_{i,0}$. Similarly, the second term models the energy contribution of all the angles formed between three atoms A-B-C, where A and C are bonded to B. For four atoms bonded together, A-B-C-D, the dihedral angle is defined as the angle formed between the A-B bond and the C-D bond viewed along the B-C bond. The energy contribution from the dihedral is represented by the third term, where ω is the torsional angle, n is the multiplicity and γ is the phase factor. The K's are the respective proportionality constants. All these terms combined describe the intramolecular (bonded) interactions. The second last term is the Urey-Bradley term, with $r_{1,3}$ the interaction distance and K_{UB} the respective force constant. The intermolecular (non-bonded) interactions are given by the last term in equation (2.2). The last term describes the van der Waals interactions modelled by the Lennard-Jones 12-6 function. σ_{ij} is the collision diameter, ε_{ij} the well depth and r_{ij} the distance between the i^{th} and j^{th} atoms. The electrostatic interactions are calculated using Coulomb's law, the last part of the intermolecular energy term. q_i and q_j are partial atomic charges on the i^{th} and j^{th} atoms respectively and ε_0 is the permittivity of vacuum.

Figure 2.1 illustrates the various terms of the potential energy.

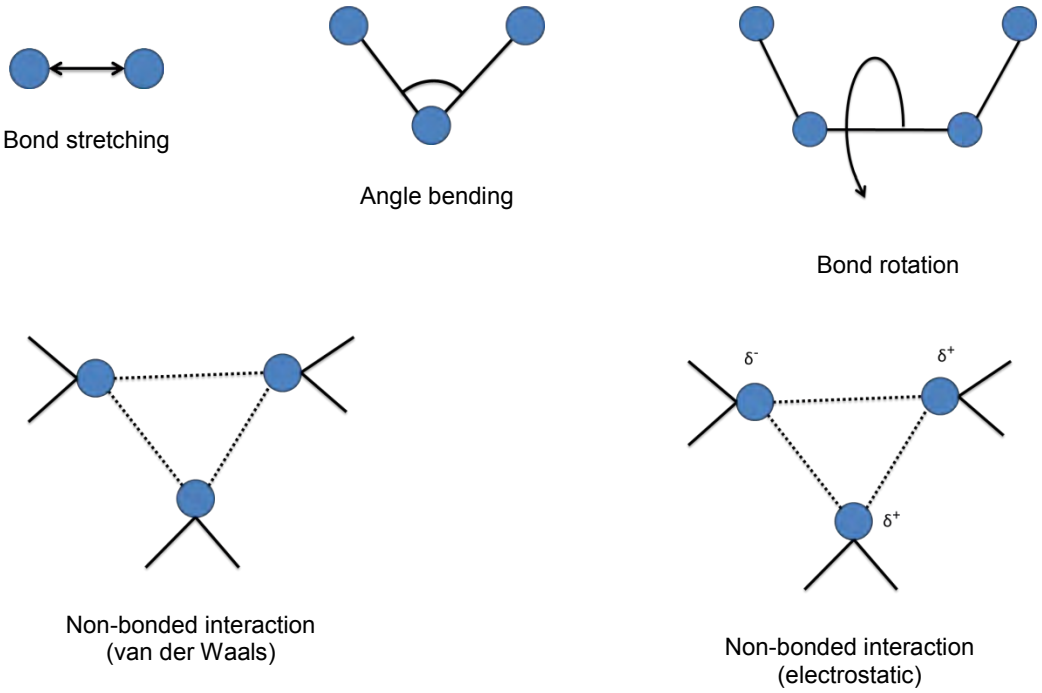

Figure 2.1: Main contributions to a molecular mechanics force field

Various force fields exist with different functional forms, some may have the same functional form but different parameters. Since these parameters are empirical the force fields can be parameterized to model specific molecular systems. Various force fields have been developed to simulate biological molecules, these include the early MM1[39] and MM2[40] force fields, AMBER,[41] GLYCAM,[42] OPLS,[43] the CHARMM[44] force fields and the CSFF[2b] force field, which is adapted from the CHARMM force fields for the study of carbohydrates. The CHARMM force field was used in this work.

2.1.2 Water models

Biological processes take place in aqueous media and as such a variety of water models have been developed for molecular modeling simulations. These range from the three site models, TIP3P[45] (three-point transferable intermolecular potential) and SCP/E[46] (extended simple point charge) to the four site, TIP4P-Ew[47] (four-point transferable intermolecular potential) and five site models, TIP5P[48] (five-point

transferable intermolecular potential). SPC/E and TIP3P models were parameterized at 298 K and have been successfully used at temperatures other than their parameterization temperature. The TIP4P-Ew and TIP5P models have been parameterized from data over a range of temperatures. The models differ in the number of interaction points and the Lennard-Jones and Coulombic terms. Figure 2.2 shows the different water models.

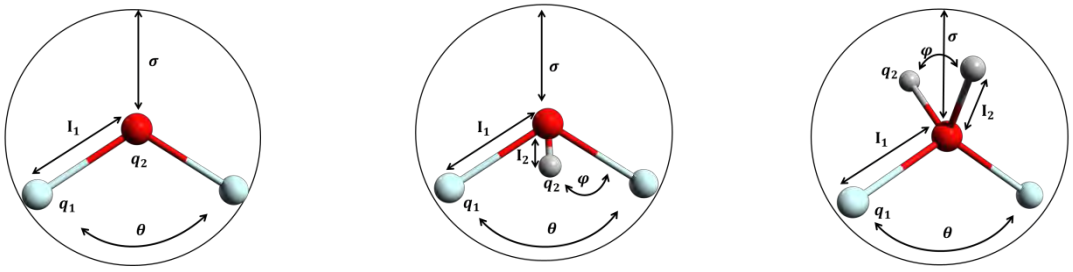

Three site **Four site** **Five site**

Figure 2.2: Schematic representation of several water models used in molecular mechanics.

A good water model should not only be able to reproduce experimental thermodynamic and kinetic properties of water but should also be able to work with other force fields to produce accurate thermodynamic and kinetic properties for solutions. These include accurate description of the solute-water interface and correct treatment of long-range interactions. The force field parameters of the models are given in Table 2.1

Table 2.1: Non-bonded parameters, geometry, and electrostatic properties of selected water models.

	ε (kJ mol^{-1})	σ (Å)	I_1 (Å)	I_2 (Å)	q_1 (e)	q_2 (e)	θ (°)	φ(°)
TIP3P	0.6364	3.15061	0.9572	-	+0.4170	-0.8340	104.52	-
SPC/E	0.65	3.166	1.0000	-	+0.4238	-0.8476	109.47	-
TIP4P-Ew	0.16275	3.16435	0.9572	0.125	+0.52422	-1.04844	104.52	52.26
TIP5P	0.6694	3.12000	0.9572	0.7	+0.2410	-0.2410	104.52	109.47

2.1.3 Molecular Dynamics

The dynamics of a system can be investigated using molecular dynamics (MD) simulations. Early MD simulations were performed using a hard-sphere model.[49] Within this model the spheres move in a straight line at constant velocity and the collisions are perfectly elastic.

MD makes use of Newton's equations of motion to determine the position of the atoms in the system. This is achieved by integrating Newton's second law of motion, (2.3) over a certain time interval, also referred to as a *timestep.*

$$\frac{\partial^2 r_i(t)}{\partial t^2} = \frac{F_i}{m_i} \tag{2.3}$$

Equation (2.3) describes the motion of a particle of mass m_i with positional coordinates $r_i(t) = (x_i(t), x_i(t), x_i(t))$ and experiencing a force F_i. A trajectory describing how the variables change with time is produced by calculating the force at time t. In a continuous potential model, the force changes with a change in the position of the atom and when the atoms that interact with it change their position,.

Finite difference methods are used for solving differential equations such as equation (2.3). The finite difference approach is utilized by several integrators such as Verlet,[50] and Velocity Verlet[51] to name a few. With this approach the positions and velocities of particles are determined by using the known positions and velocities from the previous step. A random number generator is used to assign initial velocities. The computation is performed on a step by step basis and the timestep is chosen to be less than the time taken for a molecule to travel a distance equal to its length. In situations where bonds within the molecule vibrate in a shorter time than

the timestep, algorithms such as SHAKE[52] and RATTLE[53] can be used to fix the bond lengths.

The following steps are followed when running a molecular dynamics simulation:

- *Minimization*: The initial structures are built using a molecular builder[54] or data from Neutron diffraction and X-Ray experiments can be used. They are then minimized to their lowest energy conformations. In this step any non-physical interactions (bad contacts) that can occur during solvation are removed.

- *Heating*: The low energy conformations are usually found at lower temperatures and thus it is necessary to heat the system to the appropriate temperature. During the heating stage the temperature is gradually increased to the required temperature.

- *Equilibration*: Once the system has been heated, it is simulated for a certain time period allowing it to reach an equilibrium state. The length of equilibration is largely dependent on the system size and initial structures.

- *Production*: This step involves collection of data to be used for analysis. The simulation length depends on the property under investigation.

2.1.4 Time averages and ensemble averages

With knowledge of the positions and momenta of all the particles in a system, its state can be determined. In three-dimensional space each particle will have six coordinates (three from momentum and three spatial), thus a system with N particles will have 6N coordinates. The space defined by these coordinates is called phase

space and a system can only occupy one point (phase point)inphase space at any point in time. The degrees of freedom can be expressed as:

$$X^{'} = (x_1, y_1, z_1, p_{x1}, p_{y1}, p_{z1}, x_2, y_2, z_2, p_{x2}, p_{x2}, p_{x2}, ...)$$

(2.4)

and can be more conveniently written as:

$$X^{'} = (\mathrm{p}, \mathrm{q})$$

(2.5)

where $\mathrm{p} = (p_{x1}, p_{y1}, p_{z1}, p_{x2}, p_{x2}, p_{x2}, ...)$ and $\mathrm{q} = (x_1, y_1, z_1, x_2, y_2, z_2, ...)$ with p and q being the momentum and position respectively. The average value of a property, *A*, of an *N*-particle system at equilibrium can be expressed as an ensemble average:

$$\langle A \rangle = \iint A(p^N \cdot q^N) P(p,q) dp dq$$

(2.6)

P is the probability of finding a configuration with momenta p^N and position q^N. In molecular dynamics simulation properties can be calculated as ensemble averages, i.e. an average over all phase points simulated. For a dynamic system the time average of a property is defined as the sum of all values sampled divided by the number of times it has been sampled over time. If the trajectory is sampled continuously, the average is calculated using the equation below:

$$\langle A \rangle = \lim_{t \to \infty} \frac{1}{t} \int_{t_0}^{t_0 + t} A(\tau) d\tau$$

(2.7)

From the ergodic hypothesis it followed that the above equation is independent of the choice of t_0 for a sufficiently long simulation. In such a system the temperature

(*T*), volume (*V*) and number of particles (N) are assumed to be constant. By varying which variables remain constant in the simulation different ensembles can be sampled from, namely:

- Canonical ensemble: constant *N, V, T*
- Microcanonical ensemble: constant *N, V, E* (energy)
- Isothermal-isobaric ensemble: constant *N, T, P* (pressure)

2.1.5 Periodic Boundary Conditions and Minimum Image Convention

MD simulations take place in a container of some sort. The most common periodic cells used in simulations are shown in Figure 2.3. The choice of periodic cell varies with system being studied. For spherical molecules truncated octahedron and rhombic cells may be more appropriate while for cylindrical, large molecules like DNA a hexagonal cell may be more suitable.

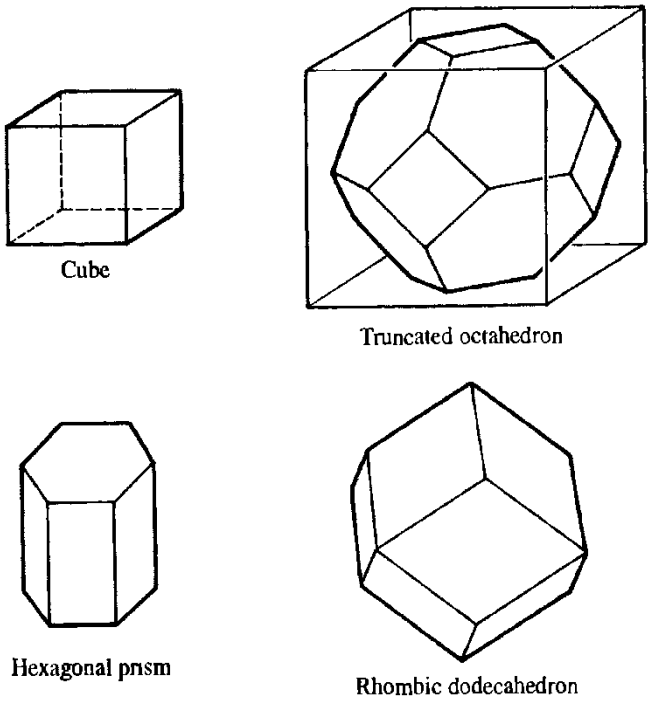

Figure 2.3: Periodic cells generally used in simulations

The way in which the molecules near the walls of the container are treated affects how macroscopic properties of the system are reproduced. The interactions of the molecules and the walls are different from those of the molecules with each other and thus to preserve the bulk properties of the molecules the interactions need to be modelled correctly. Periodic boundary conditions (PBCs) allow for simulations to be performed using a relatively small number of molecules with molecules near the walls of the container behaving as if they were in bulk liquid. This is achieved by creating an array of the simulation box (unit cell) in all dimensions to form an infinite lattice. A 2D depiction of an application of periodic boundary conditions is given in Figure 2.4 below.

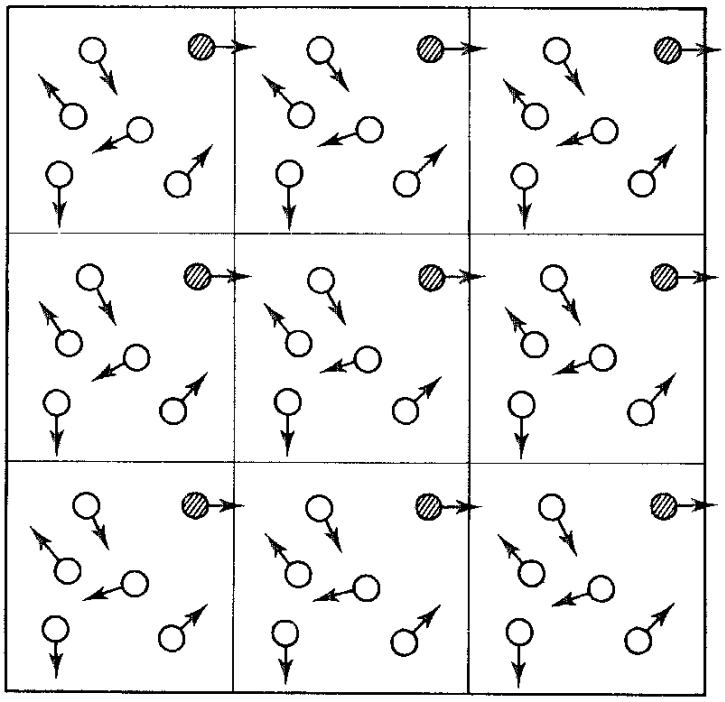

Figure 2.4: 2D representation of periodic boundary conditions from ref [36] The central box is the actual simulation box.

If an atom leaves the simulation region, it is replaced by its image atom at the position related to the exiting atom by lattice symmetry. Thus, the number of atoms in the simulation region is conserved and the mass and energy are also conserved.

A limitation of periodic boundaries is that fluctuations that have a wavelength greater than that of the periodic cell cannot be determined and as such poses a problem for simulations of liquids near the liquid-gas critical point. Full three-dimensional periodic boundaries are not always necessary, e.g. when studying properties of a system on a surface where 2 dimensional PBC would suffice.

Computation of non-bonded interactions for a system containing *N* particles scales as N^2 for a pairwise model. Due to the infinite number of replicas of the periodic cell, this dependence on system size makes the calculation very time consuming for large systems. This can be overcome by applying the *Minimum Image Convention*. With this approach only the interactions between a particle and its nearest neighbor images are calculated. An illustration of an application of the minimum image convention is given in Figure 2.5

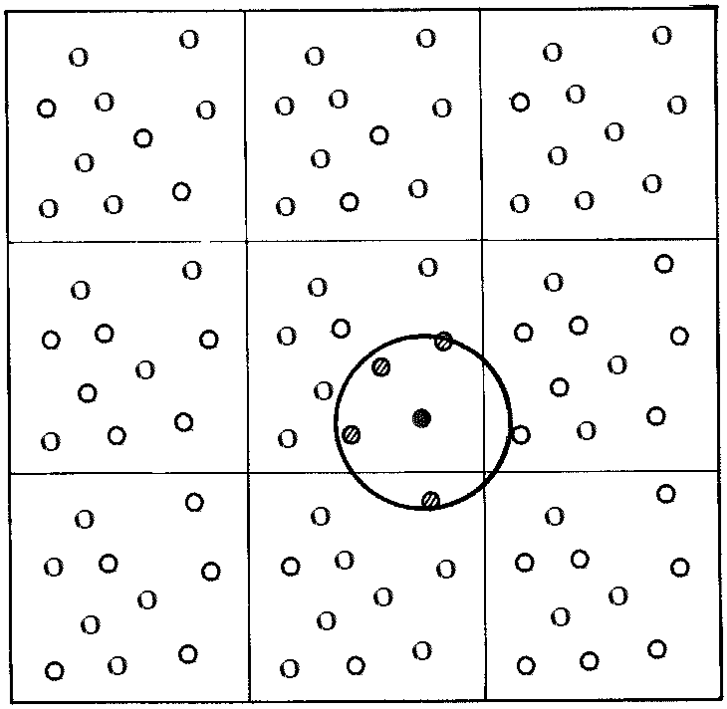

Figure 2.5: Minimum image convention. Calculation of non-bonded interactions is performed for only the particles within the circle, *non-bonded cutoff.* From ref[55]

2.1.6 Ewald summation method

In simulations of charged systems, long-range electrostatic interactions are significant. These interactions (charge-charge between ions and dipole-dipole between molecules) decay no faster than r^{-n}, where n is the dimensionality of the system. Their range is often greater than half the box length and as such when PBC are employed, long-range forces cannot be truncated without incurring errors in the calculations.[56] To overcome this, a large simulation box can be used, but this is unfeasible due to the time required to run the simulations. The time is proportional to L^6, L being the box length. Other alternatives include using techniques such as the Tree-code approach, the reaction field method, the fast multipole method and the Ewald method. The Ewald method is able to take advantage of the periodicity of the system by reorganizing the interaction sums over the periodic images of the system and thus avoiding truncation. The interaction energy is calculated over all periodic images of the simulation box. The total interaction energy is given by equation (2.8)

$$U_{qq} = \frac{1}{2}\sum_{\mathrm{n}}{}' \sum_{i=1}^{N_m}\sum_{j=1}^{N_m} \frac{q_i q_j}{4\pi\varepsilon_0 \left| r_{ij} + \mathrm{n} \right|} \qquad \textbf{(2.8)}$$

where q_i and q_j are the charges on atom i and j respectively for a simulation box of length L. The summation is over all cubic lattice points, $\mathrm{n} = (\mathrm{n}_x L, \mathrm{n}_y L, \mathrm{n}_z L)$ and the prime indicates that interactions where $i = j$ for $|\mathrm{n}| = 0$, are omitted to avoid self-interaction. This sum is conditionally convergent, i.e. the sum depends on the order in which the terms are added. To overcome this, the sum is split into two series which individually converge faster than the original. Each charge in the system is

considered to be surrounded by a charge distribution of equal magnitude but opposite sign. The Gaussian distribution is generally expressed as:

$$\rho_i(r) = \frac{q_i \kappa^3}{\pi^{3/2}} \exp(-\kappa^2 r^2)$$

(2.9)

The width of the distribution is determined by κ and r is the distance from the centre of the distribution. A cancelling distribution of the same shape and sign as the initial charge is also added. This cancelling distribution is calculated in reciprocal space. Figure 2.6 illustrates how the summation is performed. The interaction of the cancelling distribution with itself is included in the sum and thus must be corrected for.

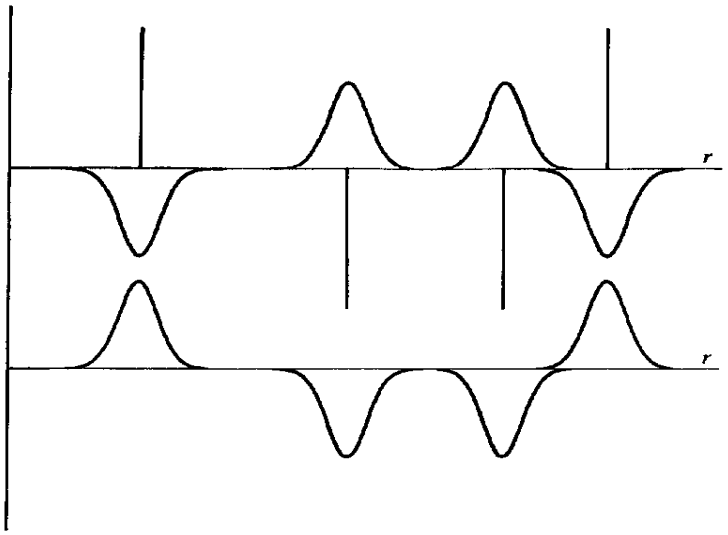

Figure 2.6: Summation of charge distributions in the Ewald method. (Top) Initial charges surrounded by a Gaussian charge distribution of equal magnitude but opposite sign. (Bottom) Cancelling distribution. Reproduced from ref [55].

The real-space summation converges rapidly for large κ and reciprocal-space summation converges rapidly for small κ, therefore the value of κ should be chosen such that both the real-space and reciprocal-space summations converge fairly rapid. The total interaction energy can now be expressed as:

$$U_{qq} = \frac{1}{2}\sum_{i=1}^{N}\sum_{j=1}^{N}\left(\begin{array}{l}\sum_{|\mathrm{n}|=0}^{\infty}{}' \frac{q_i q_j}{4\pi\varepsilon_0}\frac{\mathrm{erfc}\left(\kappa\left|r_{ij}+\mathrm{n}\right|\right)}{\left|r_{ij}+\mathrm{n}\right|}+\sum_{k=0}\frac{1}{\pi L^3}\frac{q_i q_j}{4\pi\varepsilon_0}\frac{4\pi^2}{k^2}\exp\left(-\frac{k^2}{4\kappa^2}\right)\cos(k\cdot r_{ij})-\frac{\kappa}{\sqrt{\pi}}\sum_{k=1}^{N}\frac{q^2{}_k}{4\pi\varepsilon_0} \\ +\frac{2\pi}{3L^3}\left|\sum_{k=1}^{N}\frac{q_k}{4\pi\varepsilon_0}r_k\right|^2\end{array}\right)$$

(2.10)

Here the function $\mathrm{erfc}(r)$ is the complementary error function:

$$\mathrm{erfc}(\mathrm{x}) = \frac{2}{\sqrt{\pi}}\int_{x}^{\infty}\exp(-t^2)dt$$

(2.11)

The Ewald method has been used in simulations of highly charged systems and where electrostatic effects are significant.[57] The computational cost of implementing the Ewald method is high. It scales as N^2 if κ is constant and $N^{3/2}$ if κ is allowed to vary. This can be reduced to $N\log N$ by using techniques that use the Fast Fourier Transform (FFT) to calculate the reciprocal-space summation. For the fast Fourier transform to be used, the charge on the particles must be converted to a grid-based charge distribution and thus creating discrete values of the charges at each grid point. Methods that use this technique are particle-particle-particle-mesh[58] (PPPM) and the particle-mesh Ewald method.[59] The particle-mesh Ewald method as implemented in the CHARMM program was used in all simulations in this thesis.

2.2 Quantum Mechanics

As mentioned above quantum mechanics (QM) deals mostly with the question of electronic structure. A postulate of quantum mechanics is that, for any chemical system an appropriate operator (ϑ) can be applied to the wavefunction (ψ) and return an observable property (e) of that system.

$$\vartheta\psi = e\psi$$

(2.12)

The operator that returns the energy, E, of the system is known as the Hamiltonian and equation (2.12) can be written as a well-known equation, the Schrödinger equation:

$$H\psi = E\psi$$

(2.13)

The functional form of the Hamiltonian is given in equation (2.14)

$$H = -\sum_i \frac{\hbar^2}{2m_e}\nabla_i^2 - \sum_k \frac{\hbar^2}{2m_k}\nabla_k^2 - \sum_i \sum_k \frac{q^2 Z_k}{r_{ik}} + \sum_{i<j} \frac{q^2}{r_{ij}} + \sum_{k<l} \frac{q^2 Z_k Z_l}{r_{kl}}$$

(2.14)

m_e and m_k are masses of the electron and nuclei respectively, $\hbar$ is Planck's constant divided by 2π, q is the fundamental charge, m_e is the charge of the nucleus, Z is the atomic number r_{ij} is the distance between particle i and j and ∇^2 is the Laplacian operator, which in Cartesian coordinates is expressed as:

$$\nabla_i^2 = \frac{\partial^2}{\partial x_i^2} + \frac{\partial^2}{\partial y_i^2} + \frac{\partial^2}{\partial z_i^2}$$

(2.15)

If atomic units are used equation (2.14) can be conveniently written as:

$$H = -\sum_i \frac{1}{2}\nabla_i^2 - \sum_i \sum_k \frac{Z_k}{r_{ik}} + \sum_{i<j} \frac{1}{r_{ij}}$$

(2.16)

For a given system there can be more than one eigenfucntion, ψ_i, each with its corresponding eigenvalue E_i. The set of these eigenfunctions are complete and orthonormal and thus for a one particle system in Cartesian coordinates,

$$\iiint \psi_i \psi_j dxdydz \equiv \int \psi_i \psi_j d\mathbf{r} = \delta_{ij}$$

(2.17)

2.2.1 The Variation Principle

A critical principle of quantum mechanics is the variational principle. For an arbitrary wavefunction, which can be operated upon by the Hamiltonian, the wavefunction, Φ, is a linear combination of a set of orthonormal wavefunctions, mathematically,

$$\Phi = \sum_i c_i \psi_i$$

(2.18)

In equation (2.18) the wavefunctions ψ_i, and the coefficients c_i are not known. If the energy of the wavefunction Φ, is to be evaluated, equation (2.13) takes the form

$$H\Phi = E\Phi$$

(2.19)

Combining equation (2.17) and (2.18) and applying some mathematical manipulations while taking into consideration the orthonomality of Φ, gives equation (2.19) as

$$\int \Phi H \Phi dr = \sum_i c_i^2 E_i$$

(2.20)

Equation (2.20) states that the energy of Φ is determined from the coefficients and their respective energies. From the set of all possible energy values E_i, one of them must have a smallest value. E_0.This value is referred to as the *ground state*. We know from the normality of Φ that

$$\int \Phi^2 dr = 1$$

(2.21)

and can now write

$$\int \Phi H \Phi dr - E_0 \int \Phi^2 dr = \sum_i c_i^2 (E_i - E_0)$$

(2.22)

E_0 is always greater than zero and if all coefficients are assumed to be real equation (2.22) can be rewritten as

$$\int \Phi H \Phi dr - E_0 \int \Phi^2 dr \geq 0$$

$$\int \Phi H \Phi dr \geq E_0$$

(2.23)

Equation (2.23) says that for any trial wavefunction, the corresponding energy will always be greater or equal to the ground state energy.

In the Born-Oppenheimer approximation, the square of a one electron wavefunction at a particular point is the probability of density of the wavefunction at that point. By invoking molecular orbital theory[37, 60] the charge density at a point r can be expressed as a sum over n occupied molecular orbitals of a single-determinant wavefunction:

$$\rho(r) = \sum_{i=1}^{n} |\psi_i(r)|^2$$

(2.24)

The charge density is a function of only three variables, the spatial coordinates x, y and z.

2.2.2 Antisymmetry and molecular orbitals

As stated before the Born-Oppenheimer approximation allows for decoupling of nuclear and electronic motion. The electronic Schrödinger equation is written as

$$(H_{el} + V_N)\Psi_{el}(q_i;q_k) = E_{el}\Psi_{el}(q_i;q_k)$$

(2.25)

where H_{el} only contains the kinetic energy of the electrons, the electron-nuclear interactions and the electron-electron repulsion. V_N is a constant for a specific set of nuclear coordinates. q_i and q_k are electronic and nuclear coordinates where the latter are taken as parameters. The electronic wavefunction Ψ_{el} is only dependent on the electronic coordinates.

An orbital is described as a wavefunction of a single electron. The wavefunction discussed above is a function of spatial coordinates of the electron and therefore describes the spatial orbital. This description does not take into account the spin of

the electron and therefore does not give a full description of an electron. The electron spin ,which can either be positive (spin up) or negative (spin down), denoted by α or β, describes the spin states. The spin orbital of a single electron is then given by:

$$\chi(r,\delta)$$

(2.26)

where $\delta = \alpha$ or β and r is the spatial coordinate. For convenience the spatial and spin coordinates can be written as X where:

$$\mathrm{X} = (x, y, z, \delta)$$

(2.27)

A many-electron wave function must be antisymmetric with respect to the interchange of any two electrons,[61] such that:

$$\Psi(X_1, X_2, ..., X_i, X_j, ..., X_N) = -\Psi(X_1, X_2, ..., X_j, X_i, ..., X_N)$$

(2.28)

For an N-electron wave function this antisymmetry requirement can be enforced using *Slater determinants*. The Slater determinant of an N-electron wavefunction of a closed system is given by:

$$\Psi = (N!)^{-\frac{1}{2}} \begin{vmatrix} \chi_i(X_1) & \chi_j(X_1) & \cdots & \chi_k(X_1) \\ \chi_i(X_2) & \chi_j(X_2) & \cdots & \chi_k(X_2) \\ \vdots & \vdots & & \vdots \\ \chi_i(X_N) & \chi_j(X_N) & & \chi_k(X_N) \end{vmatrix}$$

(2.29)

where $(N!)^{-\frac{1}{2}}$ is the normalisation factor. If the rows are interchanged (interchanging coordinates of electrons), then the sign of the determinant changes thereby satisfying the antisymmetry principle. If two rows are the same (two electrons with

the same coordinates) then the determinant is zero, thereby obeying Pauli's Exclusion Principle, which states that two electrons cannot occupy the same orbital.[61]

2.3 Hybrid QM/MM

Section 2.1 briefly alluded to the limitations of molecular dynamics simulations, that is, the details of electronic properties are beyond what the models can produce. Chemical reactions are characterized by breaking and forming of bonds, events that mainly involve the movement of electrons are not accurately described by classical models. Although force fields are parameterised to give the best representation of molecules, inherent properties of molecules, such as the anomeric effect in glucose, are better described by methods based on quantum mechanics. [2c, 2n, 7, 62] Pure QM simulations are computationally too expensive to run and therefore not practical for large systems. It is however possible to treat a specific region of the molecular system quantum mechanically while the rest of the system is treated by molecular mechanics methods. This combined quantum mechanical and molecular mechanical method is known as hybrid QM/MM.[63]

In a QM/MM system there is a QM region, the region of interest, and an MM region, which is usually not directly involved in the property being studied. The boundary region can be treated using periodic boundary conditions. This partitioning is illustrated in Figure 2.7

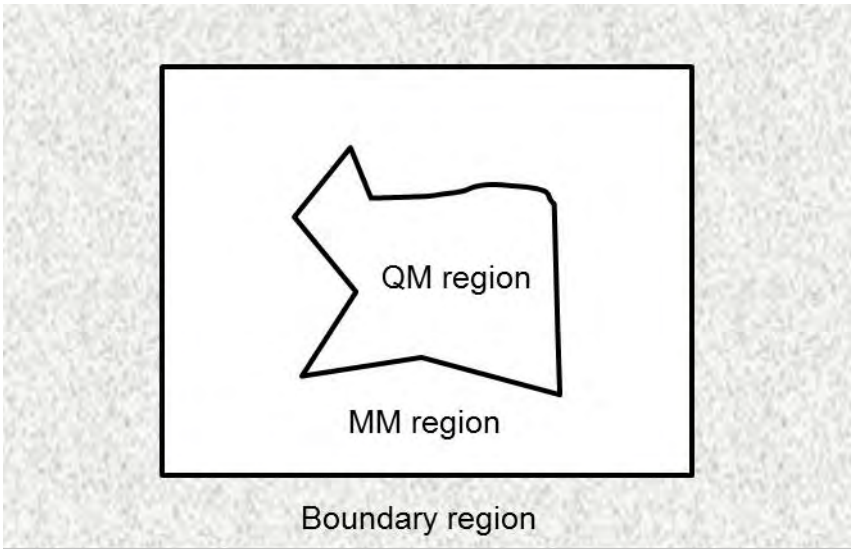

Figure 2.7: Partitioning in a QM/MM simulation model.

The Hamiltonian of a QM/MM system is described with the following equation:

$$\hat{H}_{eff} = \hat{H}_{QM} + \hat{H}_{MM} + \hat{H}_{QMM/MM} \quad \textbf{(2.30)}$$

where $\hat{H}_{QM}$ is the Hamiltonian of the isolated QM region, $\hat{H}_{MM}$ corresponds to the potential of the MM region and $\hat{H}_{QM/MM}$ is interaction of the QM atoms and the MM atoms.

SCC-DFTB approach was used to perform QM/MM simulations of sugar systems, while MD simulations were used water analysis as described in the next chapter.

2.4 Analysis Techniques

2.4.1 Time Correlation Functions and Diffusion Constants.

Correlation functions can be used to determine the relationship between two values. The correlation coefficient allows for the correlation of the values to be quantified. Correlation functions are generally expressed as:

$$c_{xy} = \frac{1}{M}\sum_{i=1}^{M} x_i y_i \equiv \langle x_i y_i \rangle$$

(2.31)

where the data set consists of M data points of x and y . Dividing the correlation function by the root-mean-square of x and y normalizes the function to a value of between -1 and +1 as given in equation (2.32):

$$c_{xy} = \frac{\langle x_i y_i \rangle}{\sqrt{\left(x_i^{\,2}\right)\left(y_i^{\,2}\right)}}$$

(2.32)

A high degree of correlation is characterized by an absolute value of 1 and 0 indicates no correlation.

Trajectories generated from MD simulations can be used to study time-dependent properties. Time correlation functions (TCFs) are used to calculate the correlation of a value of some property at a certain time to the value at a later time. The time correlation function is expressed as:

$$c_{xy}(t) = \langle x(t)y(0) \rangle$$

(2.33)

If x and y represent the same property the correlation function is called an autocorrelation function. If they represent different properties the correlation function is called a cross-correlation function. A normalized autocorrelation function will have an initial value of 1 and as $t \to \infty$ approach a value of 0 and if fluctuations of an observable with respect to its average value are considered. The correlation time is the time taken to lose correlation.

The diffusion coefficient D, can be calculated from the velocity autocorrelation function:

$$3D = \int_0^\infty dt \langle (\upsilon_i(t) \cdot \upsilon_i(0) \rangle$$

(2.34)

Equation (2.34) is an example of a Green-Kubo formula. Green-Kubo relations allow macroscopic properties to be expressed as time integrals of microscopic time-correlation functions. D can also be calculated using the mean square displacement (MSD) from the Einstein relation:

$$3D = \lim_{t \to \infty} \frac{\left\langle |r(t) - r(0)|^2 \right\rangle}{2t}$$

(2.35)

where $r(t)$ is the position of the center-of-mass of a particle at time t. Using integration by parts equation (2.34) and equation (2.35) can be shown to be equivalent.

2.4.2 Pair Distribution Functions

The structuring of a solvent about a solute atom or molecule can be determined using a pair distribution function, $g(r)$. The functional form is given by equation (2.36)

$$g(r) = \frac{V}{N^2}\left\langle \sum_i \sum_{j \neq i} \delta\left(r - r_{ij}\right) \right\rangle \tag{2.36}$$

and is defined as the probability of finding the ith and jth atom a distance r apart from each other compared to the probability for a random distribution at the same density. N is the number of atoms, V is the volume of the system and $g(r)$ is normalized so that $g(r \to \infty) = 1$.(Figure 2.8).

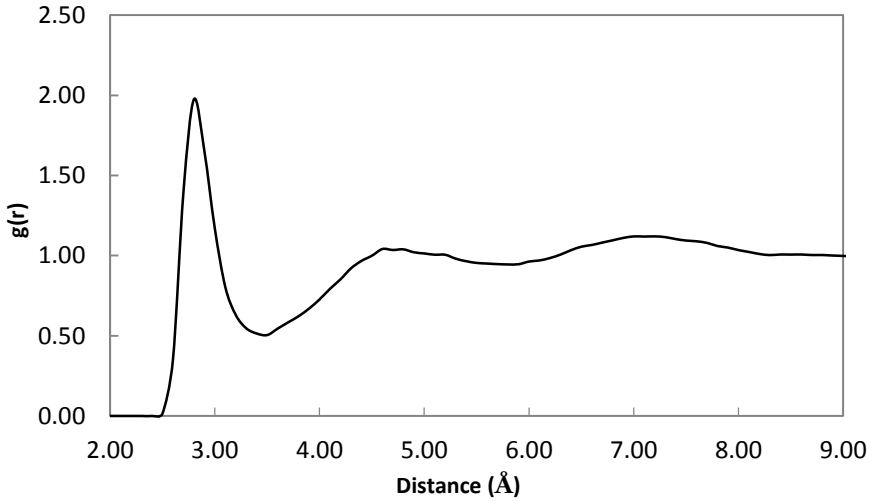

Figure 2.8: Radial distribution of cyclohexanol water calculated from a molecular dynamics simulation.

For an isotropic system $g(r)$ can be averaged over the angles without loss of information resulting in a *radial distribution function* (RDF). Not only does the RDF provide structural information, thermodynamic properties such as pressure (P), energy (E) and chemical potential (μ) can also be determined from the RDF since these properties can be defined in terms of $g(r)$.

2.4.3 Spatial Distribution Functions

To determine the anisotropic structuring around a solute spatial distribution functions (SDFs) are used. A three-dimensional water probability density can be obtained by following a procedure[64] adapted from a method used to determine the water structuring about α,α-trehalose.[65] This procedure can be summarized as follows:

1) Remove translational and rotational diffusion of the solute by selecting frames from the simulation that match a specific conformation (reference coordinate set). The length of the simulation needs to be long enough so that the number of frames in the trajectory is sufficient for obtaining a satisfactory density map.

2) A three-dimensional grid is defined with respect to the reference coordinate set. For each solvent molecule, a site of interest (oxygen atom) is 'binned' into the grid. A Gaussian function centered on the oxygen atom is used to represent the electron density of the water molecule. The Gaussian has the following form:

$$G(r_i) = elec \times \left(\frac{a}{\pi}\right)^{3/2} \times e^{-a r_i^2} \tag{2.37}$$

where $elec$ is the number of electrons associated with the atom and a is chosen so that the function drops to 10% of its maximum value at the atom's Van der Waals radius.

3) Normalization of the density is carried out according to the following equation:

$$dens_{norm}(i,j,k) = dens(i,j,k) \times \frac{n_{xbin} \times n_{ybin} \times n_{zbin}}{n_{elec} \times n_{atoms} \times n_{frames}} \quad \textbf{(2.38)}$$

where the last term contains the number of electrons in each atom, the number of atoms, the number of frames used from the trajectory and the number of x, y and z bins used in the binning.

Chapter 3 Water structure and dynamics

Introduction

The structure of water is often described in terms of the relative positions of the water molecules and their motion. Properties such as viscosity, dielectric relaxation time and self-diffusion depend on the rate of molecular translation and reorientation. Various experiments [24a, 24c, 66] have shown that a single water molecule is a double donor and double acceptor with an average of 3.5 hydrogen bonds. The structuring of water molecules around solutes occurs by water reorientations. These changes occur as the water hydrogen bond network adapts to the presence of solute molecules. Different mechanisms have been suggested to explain the phenomenon of water reorientation in liquid water. This chapter explores a mechanism that has been recently reported in literature and lays a foundation for studying the motion of water around various hexacyclic molecules.

3.1 Hydrogen Bond Exchange

3.1.1 Orientational Defects Model

A model proposed in the early days is the orientational defects model, it is based on the reorientation mechanism in ice.[67] In this mechanism the reorientation occurs by a 120° rotation of a water molecule's OH bond towards the O-H··O axis of the neighboring water molecule (Figure 3.1a). This results in the rotating molecule's hydrogen atom facing a hydrogen atom of the neighboring water molecule and is known as the D-defect (Figure 3.1b). The oxygen atom of the rotating water molecule ends up facing the oxygen of its initial hydrogen bond acceptor (Figure 3.1b) and this is the L-effect. The initial H-bond acceptor molecule rotates to adjust to the change in the H-bond network (Figure 3.1c). As each water molecule

responds to the rotations of their neighboring water molecules, the defects occur at different places in the H-bond network.

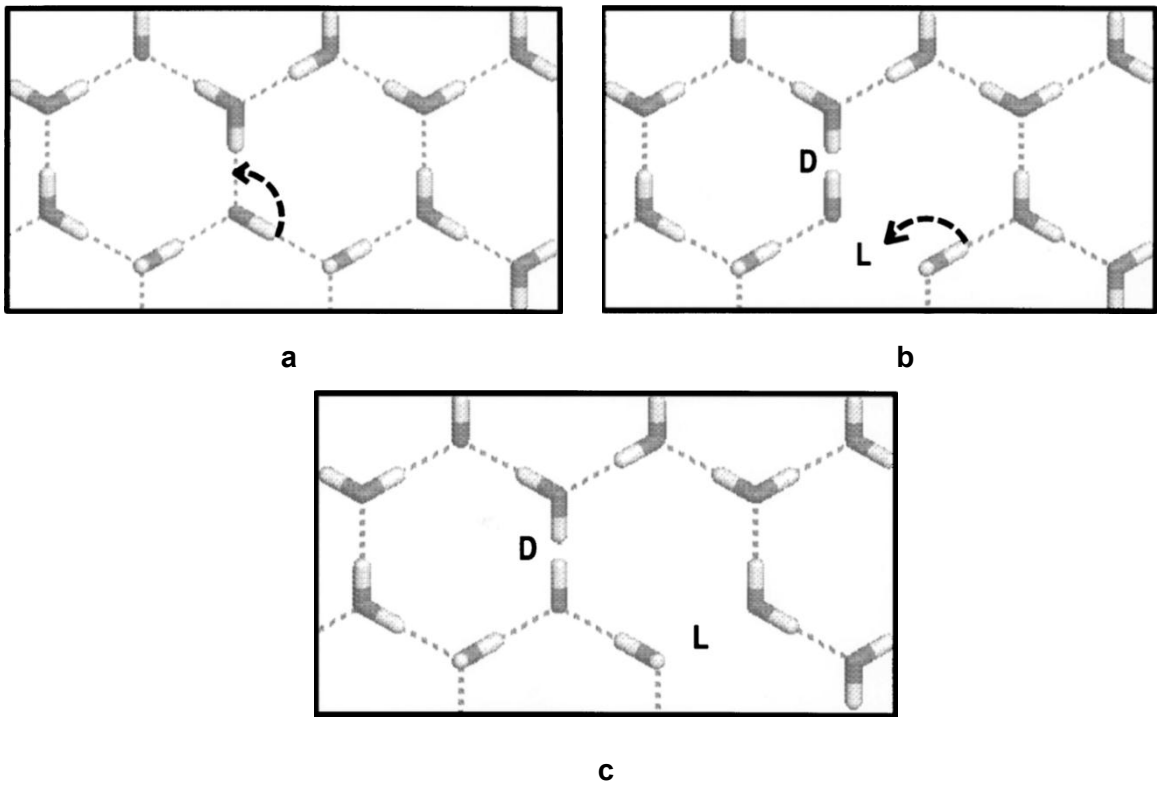

Figure 3.1: Representation of reorientation of water molecules as described in the orientational defects model (as illustrated in ref [22]).

The actual configuration of the neighboring water molecules in the presence of the defects is not known. It is however expected that there will be repulsion between the H···H and O···O pairs. Although there is no direct evidence of this mechanism, the theory has been shown to be in accord with experimental data.[68] Various other mechanisms have been proposed and are discussed in more detail in ref [22].

3.1.2 Molecular Jump Mechanism

A mechanism of interest is the molecular jump mechanism (MJM) proposed by Laage et al.[69] Through theoretical studies Laage et al. have elucidated the sequence of events involved in breaking and forming of hydrogen bonds in liquid water. Two-dimensional infrared experiments have also been used to support the

existence of such a mechanism.[70] The behavior of molecules around hydrophobic solutes can also be explained by this mechanism.[71] Rezus and Bakker[72] reported that water molecules in the first hydration shell of hydrophobic solutes are immobilized. Laage and Hynes showed that by considering transition state excluded volume within the context of MJM the slowdown of water mobility can be predicted and they have also explained why the solute has little effect on the immobilization of water around it.[71]

The MJM model suggests that water reorientations occur via large angular jumps. Figure 3.2 shows how the reorientation occurs.

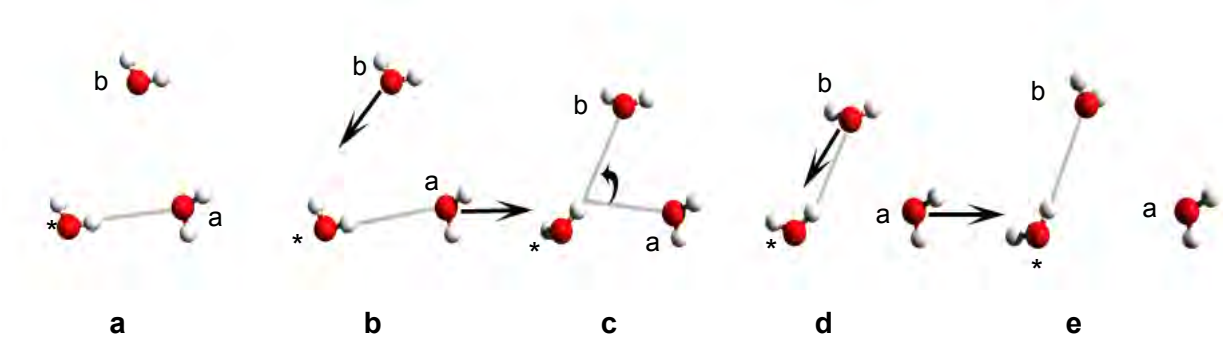

a **b** **c** **d** **e**

Figure 3.2: Water reorientation as explained by the Molecular Jump Mechanism. The arrows indicate the direction of motion of the molecules.

The molecules are initially in their tetrahedral configuration (Figure 3.2a) with O_a in the first hydration shell of O* and O_b not interacting with O*. Due to fluctuations in the hydrogen bond network O_a becomes overcoordinated and moves away from O* while O_b becomes undercoordinated and starts moving towards O* (Figure 3.2b). This motion continues until O_a and O_b are equidistant from H* and a bifurcated hydrogen bond is formed (Figure 3.2c), this configuration is referred to as the *transition state*. In Figure 3.2d the initial O*–H*···O_a bond breaks while the O*–H*···O_b bond remains intact and is reinforced by O* and O_b moving closer together. The rotation of H* from O_a to O_b is characterized by a large angular jump of 66° ~ 68°.[69]

This mechanism has been employed to study water reorientation around anions[73] and the reorientation mechanism was found to be similar to that occurring in pure water. At the transition state, the $Cl^-\cdots H–O$ bond is weaker and longer than the $O\cdots H–O$ bond. The transition state configuration is achieved when the $Cl^-\cdots H–O$ and $O\cdots H–O$ hydrogen bond interaction energies are of equal magnitude, instead of hydrogen bond lengths being equal as in the case of liquid water.

The CHARMM program was used to perform molecular dynamics simulations using the TIP4P-Ew[47] water model in a cubic simulation box containing 512 water molecules and the box length set to 24.8026 Å. Periodic boundary conditions were applied. The SHAKE[74] algorithm was used to fix hydrogen-oxygen bonds. The trajectory was propagated at 298.15 K for 1 ns in the isothermal-isobaric ensemble (NPT). Long-range forces were treated using Ewald summation.[59]

The objective was to reproduce the results reported by Laage et al.[69] (the SPC-E[46] water model was used in their study) and to validate the method used in this thesis to investigate hydrogen bond exchanges around various molecules.

3.1.3 Results

3.1.3.1 Motion and Local Structure of Water

The self-diffusion was calculated using the mean square displacement and system size dependence corrected using the equation reported by Yeh and Hummer[75]

$$D = \lim_{t\to\infty} \frac{\left\langle \left| r(t) - r(0) \right|^2 \right\rangle}{6t} + \frac{2.837297 k_{\mathrm{B}} T}{6\pi\eta L} . \qquad (3.1)$$

where T is the absolute temperature, η the shear viscosity of water, k_B the Boltzmann constant and L the length of the cubic simulation box. A value of 2.69 x10^{-5} cm^2/s was obtained from the slope of the linear region of the graph in Figure

3.3. This is in good agreement with reported experimental values of 2.30 x10^{-5} cm^2/s – 2.50 x10^{-5} cm^2/s in the literature.[76]

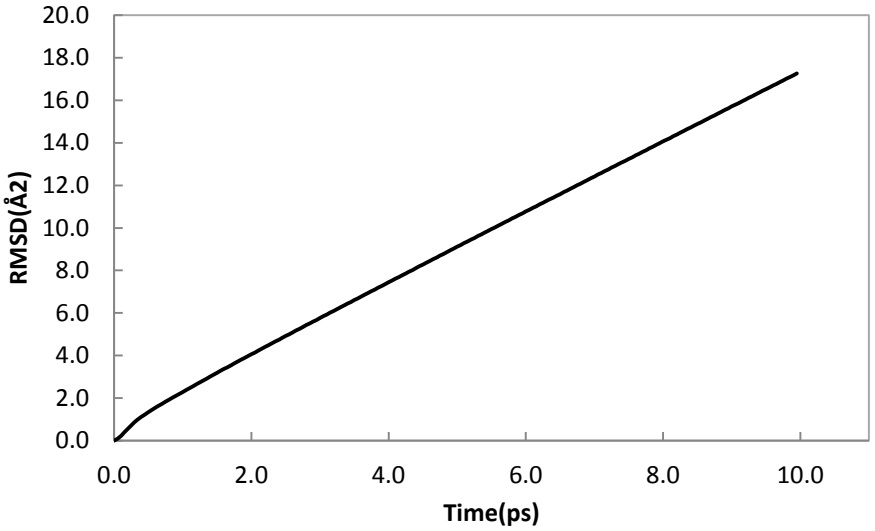

Figure 3.3: Mean square displacement of water as a function of time.

A plot of the oxygen-oxygen radial distribution function shows the first peak appears at ~2.8 Å (Figure 3.4), this is in good agreement with results from previous studies.[21, 77] Integration under the first peak gives 3.9 as the number of water molecules in the first hydration shell of a single water molecule. The peak at ~2.8 Å is indicative of short-range order in the liquid while at longer distance (>8 Å) there is disorder, $g_{oo}(r) \sim 1$.

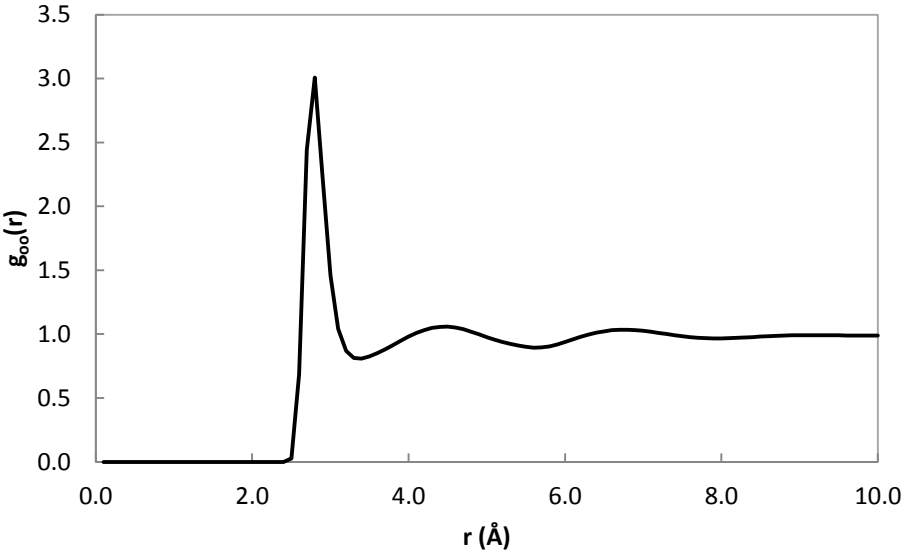

Figure 3.4: O-O radial distribution function of water at 298.15 K

3.1.4 Water Reorientation

The reorientation of water molecules can be studied by defining geometric coordinates (Figure 3.5) that can be monitored during a simulation.

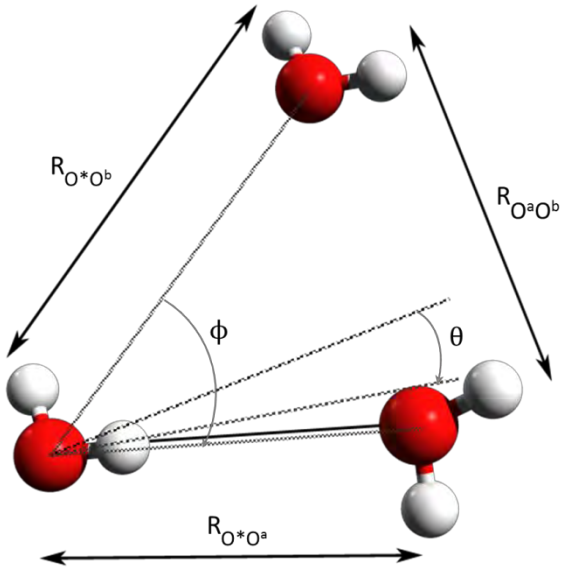

Figure 3.5: Coordinates used to monitor the hydrogen bond exchange.

$R_{O^*O_a}$, $R_{O^*O_b}$ and $R_{O_aO_b}$ are the oxygen-oxygen distances between the reference molecule (O*) the initial hydrogen bond acceptor (O_a), the new hydrogen bond acceptor (O_b) and between O_a and O_b, respectively. θ is the angle between the projection of the OH* vector onto the $O^*O_aO_b$ plane and the $O_aO^*O_b$ angle bisector . Defining θ in this way makes it independent of the motion of H* out of the $O^*O_aO_b$ plane and the bending of the $O^*O_aO_b$ angle. ϕ is the $O^*O_aO_b$ angle. Figure 3.6 shows the calculated oxygen-oxygen distances and the θ angle trajectories. The average distance between O* and O_a is 2.89 Å before the jump and 3.53 Å after the jump while that between O* and O_b is 3.58 Å before the jump and 2.86 Å after the jump.

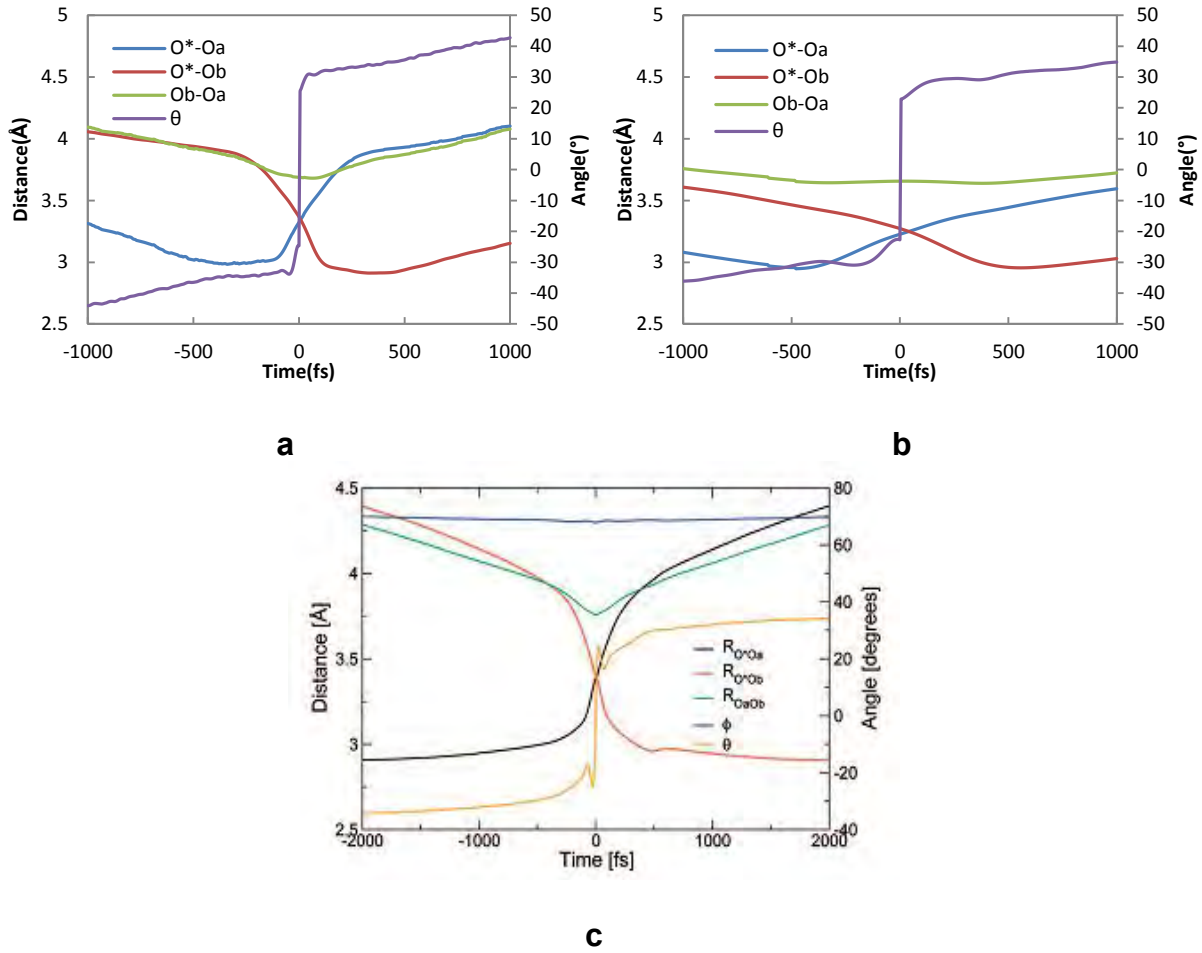

Figure 3.6: Time evolution of the H-bond exchange geometric coordinates as described in Figure 3.5 calculated from (a) the SPCE water system , (b) the TIP4P-Ew water model and (c) reproduced from ref [78].

The plots clearly show a significant change in distances at $t = 0$. The lines cross at ~3.20 Å confirming the formation of a bifurcated hydrogen bond resulting in a five-coordinate water molecule. The decrease in $O^*\cdots O^b$ distance before the jump and increase in $O^*\cdots O^a$ distance after the jump happens in approximately 200 fs. The rotation angle was determined to be ~65.66° and 74.75° for the TIP4P-Ew and SPC/E water models, respectively. The TIP4P-Ew angle is closer to the reported value of ~66° - 68°.[69a]

Figure 3.6c shows the results obtained by Laage and Hynes. From a comparison of Figure 3.6a, Figure 3.6b and Figure 3.6c it can be seen that the general motion of the water molecules is captured in both Figure 3.6a and Figure 3.6b.

Water reorientation has been shown to occur via the molecular jump mechanism using the TIP4P-Ew water model. This is consistent with the observations made by Laage et al. in that the mechanism is not dependent on the water model used.[69a] The calculated rotation angle is in agreement with the reported value. This verifies the method used in this thesis to study water reorientations.

Chapter 4 Water dynamics in hydration shells of selected monosaccharides

Introduction

Biological processes essential for life take place mostly in aqueous media. Water is able to simultaneously form hydrogen bonds as a donor and acceptor and thus has unique properties as solvent and pure liquid.[21, 79] These properties influence how water interacts with solute molecules. Water molecules in hexagonal ice have a tetrahedral structure, this structure is retained when water melts although it is not as ordered as in ice.[22] When a solute is introduced into liquid water, the tetrahedral structuring is perturbed. The interaction of water with the solute influences the extent of perturbation and the resulting water structure. A key to understanding some of the biological processes lies in understanding how solutes interact with water. Various experimental techniques such as depolarized Rayleigh scattering,[10] quasielastic neutron scattering,[12] Nuclear Magnetic Resonance (NMR)[80], terahertz dielectric relaxation spectroscopy,[81] terahertz absorption spectroscopy,[13] and infrared spectroscopy,[14, 70a, 82] have been employed to study the structure and dynamics of water around biomolecules. Water molecules proximal to the solute molecule lose their tetrahedral arrangement and form a new structure around the solute.

Molecular dynamics simulations have also shown the existence of hydration layers around biomolecules[17, 20b, 83] and that the dynamics of water around these complexes are affected by their topology.[17, 20b] In carbohydrate systems, the hydroxyl groups impose a tetrahedral-like ordering of water molecules interacting with them. This is a result of water molecules sitting on sites around the hydroxyls that minimises steric interactions.[17] It has been shown for cyclic systems that the hydration of a solute is heavily influenced by its conformational flexibility i.e.

molecules with very flexible cyclic frames have a lower hydration number than those with more rigid frames and adding an oxygen atom to an all carbon cyclic frame results in a more rigid frame.[16] The motion of water is slowed down in the presence of solutes, both translational and rotational motion is affected.[2e, 13, 20a, 20c] Laage et al. have shown that water reorientation occurs via the molecular jump mechanism[69] and have used this mechanism to explain water dynamics at the solute-water interface.[71, 84] In the molecular jump mechanism, hydrogen bond exchange takes place via large angular jumps of the rotating water molecule.

This mechanism gives detailed information on the dynamic motion of water. This forms the basis for studying the dynamics of water around monosaccharides in solution.

SCC-DFTB QM/MM simulations were performed in the isothermal-isobaric ensemble (NPT) at 298.15 K. The solute molecules were selected as the QM region and solvent molecules treated with classical MM. Periodic boundary conditions were applied in a cubic box of length 24.3373 Å and long range electrostatic interactions were treated with the particle-mesh Ewald summation technique[59, 85] as implemented in the CHARMM[1a] program. The TIP4P-Ew[47] water model was used together with the CHARMM force field parameters.[44b] The mio-0-1 parameters were used in the simulations and the hydrogen bonding treatment was improved by using the HBON keyword. The SHAKE[74] algorithm was used to constrain bonds involving hydrogen and heavy atoms (oxygen and carbon). The systems were equilibrated for 2ns and further 2ns production trajectories were generated.

The numbering scheme for the hexacyclic systems followed is as described in Chapter 2 and is presented in Figure 4.1.

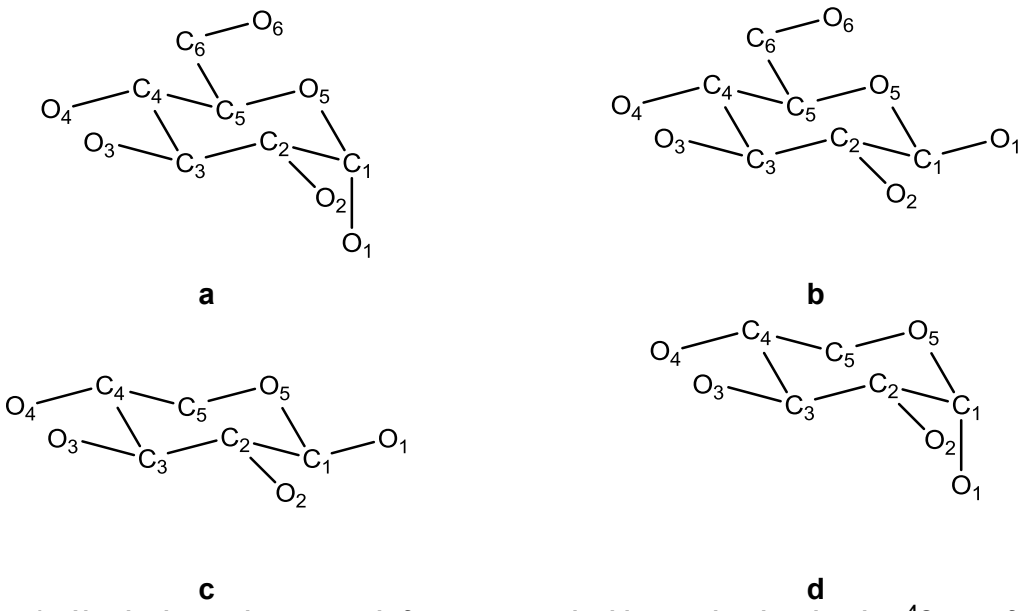

Figure 4.1: Numbering scheme used for monosaccharides molecules in the $^4C_1$ conformation. (a) β-D-glucopyranose (b) α-D-glucopyranose (c) β-D-xylopyranose (d) α-D-xylopyranose. Hydrogen atoms are omitted. This numbering scheme is used in subsequent chapters.

4.1.1 Solute dynamics

The solubility of a molecule can be attributed to the inherent nature of the molecule and the solvent system. Addition of hydroxyl groups on hexacyclic molecules only improves their solubility to a small degree. It is their conformational flexibility that plays an important role in the hydration of the molecules.[16] The motion of these molecules is investigated with a view to further understand their hydration.

4.1.1.1 Solute diffusion

The translational diffusion of the hexacyclic molecules was calculated from the mean square displacement as described in Section 2.1.4. The diffusion constants of the molecules calculated from QM/MM simulations are reported in Table 4.1.

Table 4.1: Translational diffusion constants of the monosaccharides. The standard error is given in parenthesis.

Solute	D_{calc} (x10^{-5}cm^2/s)	D_{exp} (x10^{-5}cm^2/s)
β-D-glucopyranose	0.17(0.01))	0.68[86]
α-D-glucopyranose	0.96(0.05)	
β-D-xylopyranose	0.04(0.01)	0.75[87]
α-D-xylopyranose.	0.16(0.05)	

The diffusion rates for the β-anomers are slower than α-anomers in both glucopyranose and xylopyranose. This suggests that water is interacting more favourably with the β-anomers. A slower diffusion rate also suggests that long lived hydrogen bonds may be formed between the hydroxyls and water molecules. The diffusion rate has been linked to the ring pucker rate which is also linked to the solubility of the molecules. It has been shown that the slower the ring puckers, the longer the hydrogen bonds formed[16]. The interactions between water and the sugar molecules is described in the sections that follow. The experimental diffusion rates indicate that glucopyranose has more favoured interactions that xylopyranose and hence the slower rate. This is in agreement with the trend observed for β and α-anomers of glucopyranose and xylopyranose. However, this trend is reversed when the average diffusion rates are considered.

4.1.2 Solvent dynamics

4.1.2.1 Water structure around monosaccharide molecules

The most common methods of studying structure are radial distribution functions (RDFs), and spatial distribution functions (SDFs). RDFs provide details about the average molecular organization. For an anisotropic description SDFs are employed. These methods give an average static picture of the water structure around the solute. RDFs calculated from each system are shown in Figure 4.2

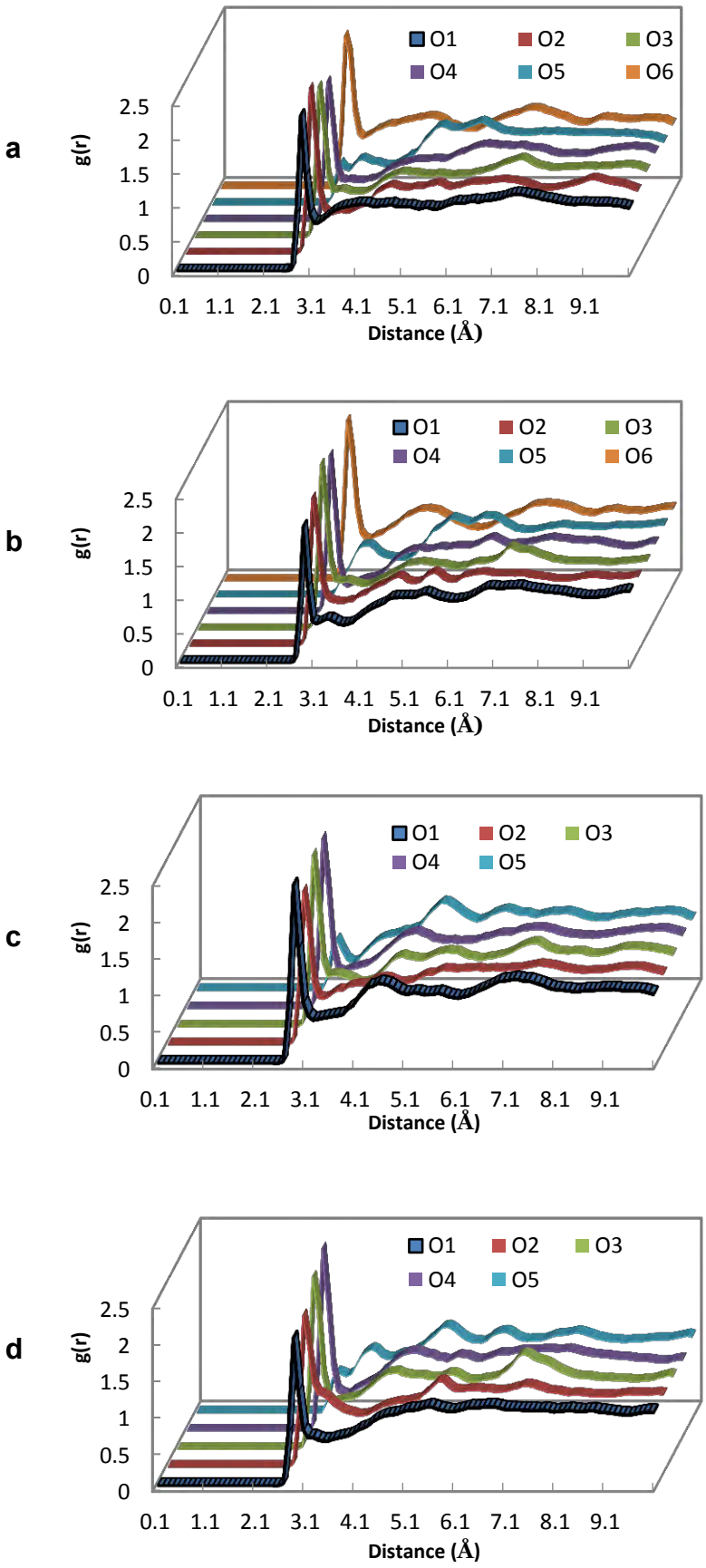

Figure 4.2: O-O RDFs calculated for each hydroxyl oxygen of the monosaccharides molecules, (a) β-D-glucopyranose, (b) α-D-glucopyranose, (c) β-D-xylopyranose and (d) α-D-xylopyranose.

Only the first hydration shells are well defined for all systems. The O-O distance of the first peak of each oxygen atom is ~2.8 Å except for O5 which occurs at ~3.5 Å in α-D-glucopyranose and in α-D-xylopyranose. The height of the O5 peaks are also lower than the other hydroxyl peaks. The O1 peak is higher in both the β-anomers. This suggests that water molecules interact differently when the hydroxyl on the anomeric carbon is in the axial position. To further investigate the structure of water, SDFs of the molecules were calculated.

The structure of water has been discussed in Chapter 3. Svishchev and Kusalik have shown that the local ordering around a water molecule extends to the second hydration shell.[77a] They have also demonstrated by means of water probability densities the relative positions of water molecules next to one another. In the case of the pyranose based molecules, the ordering is more complex. This is due to the topology of the molecule and steric effects. When two hydroxyl groups are adjacent, a half moon shaped water probability density is observed (Figure 4.3). This half moon shape is also seen for densities around the ring oxygen across all systems but α-D-xylopyranose. In the β-D-glucopyranose system there is a high density between O1, O5 and O6 which is neither seen in α-D-glucopyranose nor xylopyranose anomers. The difference between α-D-glucopyranose and β-D-glucopyranose is due to the hydroxyl group on the anomeric carbon in α-D-glucopyranose being in the axial position. The presence of this high density around the O1-O5-O6 region results in β-D-glucopyranose having the largest overall water probability density.

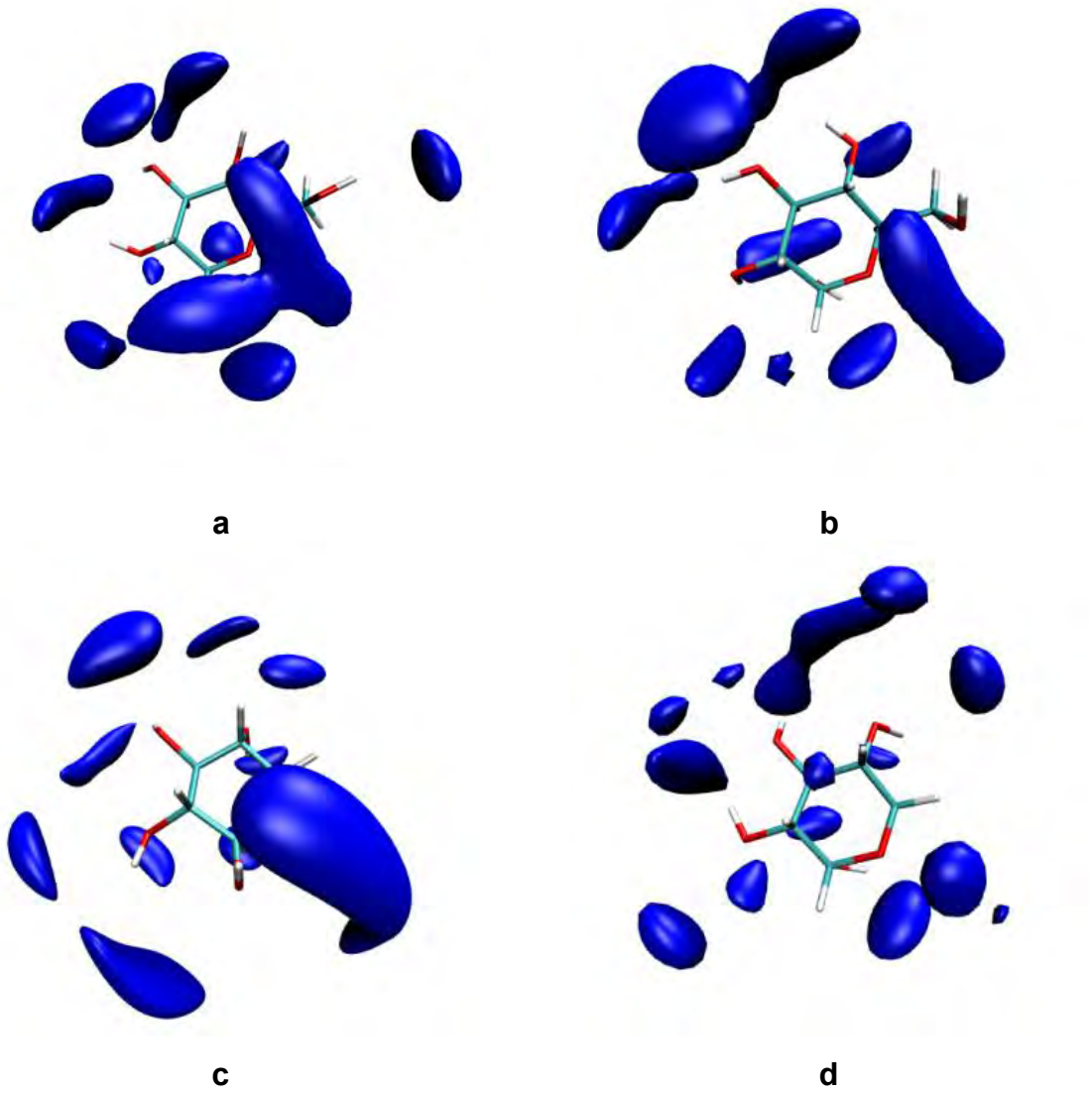

Figure 4.3: SDFs of the monosaccharides at 50% above bulk density. (a) β-D-glucopyranose, (b) α-D-glucopyranose, (c) β-D-xylopyranose and (d) α-D-xylopyranose.

When evaluating the β-anomers of glucopyranose and xylopyranose it can be seen that high density in the O1-O5-O6 region also owes its presence to the primary alcohol. The SDFs results suggest that water structuring is significantly affected by the position of the hydroxyl on the anomeric carbon and the primary alcohol.

4.1.2.2 Diffusion of water in hydrations shells of sugar molecules

Both translational and rotational diffusion constants were calculated for water in the hydration shells of the monosaccharide molecules. These were calculated for water molecules around each hydroxyl group on the molecule. Only water molecules that are within 3.4 Å of the solute oxygen are selected. The translational and rotational diffusion constants are given in Table 4.2 and Table 4.3 and respectively.

Table 4.2: Translational diffusion constants (x10^{-5} cm^2/s) of water around hydroxyl groups on sugar molecules, calculated from mean-square displacement with the standard error of the mean in parenthesis.

	β-D-glucopyranose	α-D-glucopyranose	β-D-xylopyranose	α-D-xylopyranose
O1	0.22(0.002)	0.23(0.002)	0.17(0.05)	0.25(0.002)
O2	0.23(0.003)	0.20(0.001)	0.15(0.04)	0.24(0.005)
O3	0.23(0.001)	0.25(0.001)	0.16(0.05)	0.23(0.002)
O4	0.22(0.005)	0.22(0.001)	0.24(0.01)	0.24(0.009)
O5	0.21(0.004)	0.17 (0.002)	0.18(0.05)	0.30(0.009)
O6	0.23(0.003)	0.23(0.001)	-	-
Average	0.23	0.22	0.18	0.20

Table 4.3: Rotational relaxation times (ps) of water around hydroxyl groups on sugar molecules calculated along the OH bond vector.

	β-D-glucopyranose	α-D-glucopyranose	β-D-xylopyranose	α-D-xylopyranose
O1	0.68	0.72	0.70	0.76
O2	0.74	0.72	0.72	0.70
O3	0.66	0.72	0.69	0.75
O4	0.73	0.74	0.74	0.74
O5	0.57	0.54	0.58	0.47
O6	0.69	0.76	-	-
Average	0.68	0.70	0.69	0.68

From Table 4.2, it can be seen that for glucopyranose, the average translational diffusion rate of water around the β-anomer is higher than for the α-anomer. In both anomers, the relaxation rate around O5 is slower. In the case of xylopyranose, the average water relaxation rate is higher for the α-anomer. The translational diffusion rates around O5 are also reversed, where around the α-anomer, water diffuses at a

higher rate. Perusal of Table 4.3 reveals that the trend observed for average reorientation rate around both sugars is reversed. In both anomers of glucopyranose, water molecules around O5 have a slower reorientational rate than around the hydroxyl groups. The same is also observed for the xylopyranose anomers. As with the translational diffusion rates, water molecules around O5 on α-D-xylopyranose reorientate much faster compared to water around O5 on glucopyranose and β-D-xylopyranose. This trend corresponds to the water densities around O5 for each of these molecules (Figure 4.3). This indicates that the rotational motion of water molecules around these sugar molecules is affected to a larger degree than the translational motion is, by the topology of the sugar molecules.

4.1.2.3 Water reorientation around hydroxyl groups on monosaccharides

To further investigate the motion of water molecules interacting with the sugar molecules, an approach similar that used in pure water was taken. The definition of the geometric coordinates used to study the rotational motion of water interacting with hydroxyls on the sugar molecules is given in Figure 4.4.

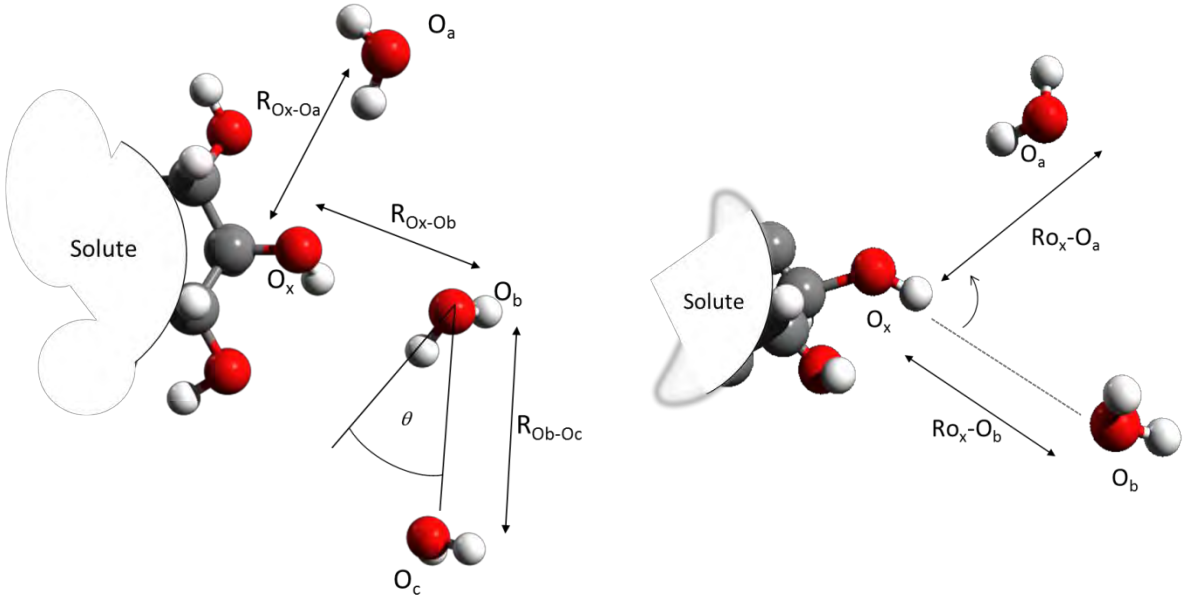

a **b**

Figure 4.4: Geometric coordinates used to monitor hydrogen bond exchange around hydroxyl groups on hexacyclic molecules.

O_b is the rotating molecule, O_a the molecule initially hydrogen bonded to the hydroxyl O_x, and O_c is the molecule initially hydrogen bonded to the rotating molecule, O_b. θ is defined as the angle formed by the projection of the O_bH bond onto the plane formed by $O_xO_bO_c$ and this gives a measure of how large a jump O_b makes during reorientation. This type of reorientation is referred to as *water-centred*. The hydrogen bond exchnage can also occur when the hydroxyl group (O_x), is donating its hydrogen atom to a water molecule (O_b), as is illustrated in Figure 4.4b. The hydrogen atom rotates towards another water molecule (O_a), to form a new hydrogen bond and this type of reorientation is referred to as *hydroxyl-centred.* Both the water-centred and hydroxyl-centred rotation involve a water to hydroxyl (WTH) rotation.

Following the motion of the water molecules, it was found that water reorientation in the hydration shells of the sugar molecules occurs via the molecular jump mechanism similar to that in pure water. However when there are two hydroxyl

groups adjacent to one another, there are two mechanistic pathways a rotating water molecule can follow.

In the first case (Figure 4.5a), a rotating water molecule breaks its hydrogen bond with a water molecule and forms a new hydrogen bond with a hydroxyl group. A similar observation was made by Vila Verde and Kramer[2e] in an experiment where they studied water dynamics around disaccharides. Alternatively a rotating water molecule can break its hydrogen bond with one hydroxyl group and form a new hydrogen bond with an adjacent hydroxyl group (Figure 4.5b). The rotation of water molecules between hydroxyl groups is also characterized by a large angular jump. Similar intramolecular hydrogen bond exchanges have been reported in literature.[88]

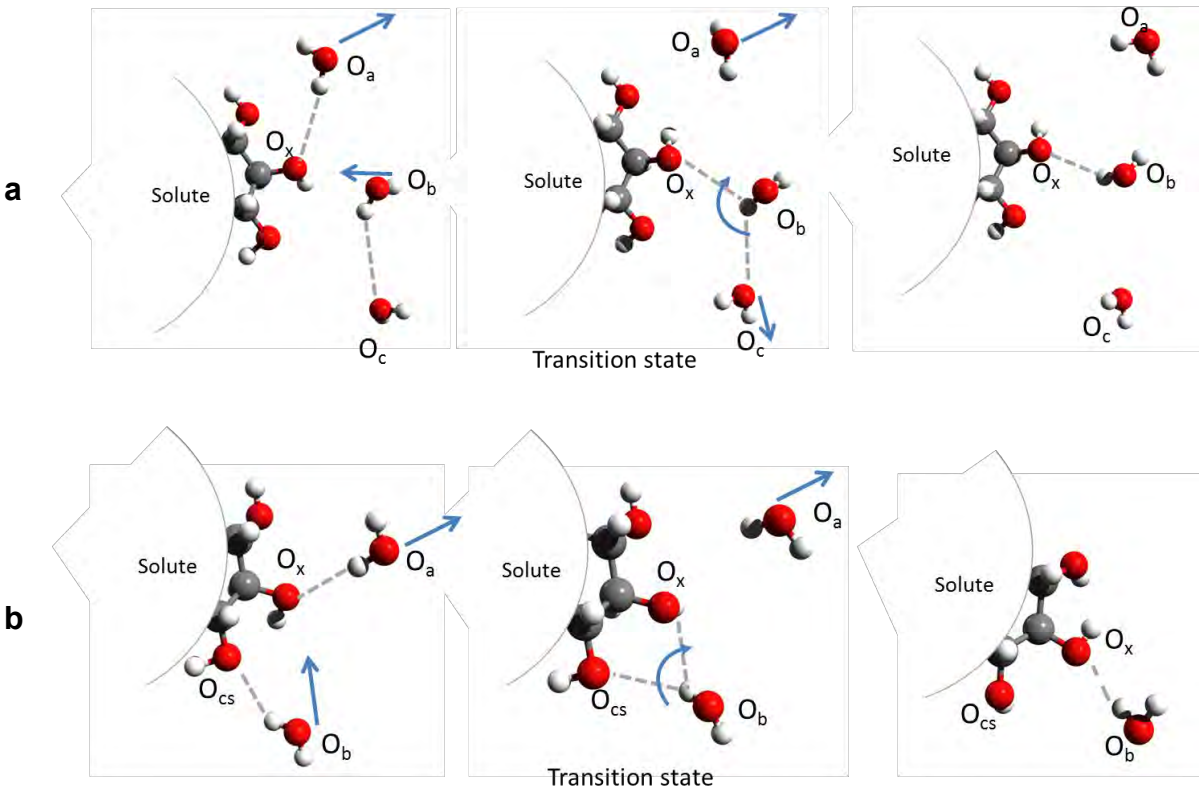

Figure 4.5: Two pathways for hydrogen bond exchange around hexacyclic molecules. (a) Pathway observed for all systems and (b) observed only when two or more hydroxyl groups are tethered to adjacent carbon atoms on the pyranose frame.

Figure 4.5a illustrates WTH exchanges and the sequence of events correspond to those in pure water. It starts with a weakening of the $O_aH\cdots O_x$ bond. A water molecule, O_b approaches O_x, the hydroxyl oxygen. The transition state is reached when the rotating water molecule's hydrogen atom H_b, is equidistant from O_x and O_c and a birfurcated hydrogen bond is formed. The $O_aH\cdots O_x$ and $O_bH\cdots O_c$ hydrogen bonds break and a new hydrogen bond forms, $O_bH\cdots O_x$. The events in Figure 4.5b are similar to the WTH pathway, the only difference is that instead of a water-water hydrogen bond breaking, a water-hydroxyl ($O_bH\cdots O_{cs}$), hydrogen bond breaks resulting in a hydroxyl to hydroxyl (HTH) rotation.

The values of the rotation angle of the two pathways are given in Table 4.4 and Table 4.5 for the WTH and HTH rotations.

Table 4.4: WTH rotation angles (in degrees) calculated for each hydroxyl of the sugar molecules.

	β-D-glucopyranose	α-D-glucopyranose	β-D-xylopyranose	α-D-xylopyranose
O1	73.45	73.70	76.26	71.02
O2	72.14	73.48	79.14	56.97
O3	75.39	74.92	77.54	77.87
O4	79.69	79.69	71.77	51.16
O5	82.27	77.12	60.92	66.92
O6	68.88	73.98	-	-
Average	75.30	75.48	73.13	64.79

Table 4.5: HTH rotation angles (in degrees) calculated for each hydroxyl of the sugar molecules.

	β-D-glucozpyranose	α-D-glucopyranose	β-D-xylopyranose	α-D-xylopyranose
O1	40.42	46.36	42.03	32.15
O2	39.43	43.20	54.53	34.20
O3	39.59	44.33	49.04	33.94
O4	51.78	51.78	53.84	36.37
O5	48.03	50.90	56.80	35.06
O6	44.88	47.58	-	-
Average	44.02	47.36	51.25	34.34

It can be seen in Table 4.4 that the average WTH rotation angles are larger than those calculated for pure water (~66°–68°[69]) with the exception of α-D-xyloopyranose. The overall average rotation angle for glucopyranose and β-D-xylopyranose are in the range of 72° – 75° while that of α-D-xylopyranose is smaller.

The HTH angles for all the molecules are smaller than their corresponding WTH values. This is consistent with the suggested pathways in that for the HTH rotations, hydroxyl groups are situated close to one another and the water molecule travels a shorter distance when rotating and hence a much smaller change in angle. This can

be seen in the plots of the geometric coordinates used to monitor the hydrogen bond exchanges shown in Figure 4.6 – Figure 4.9

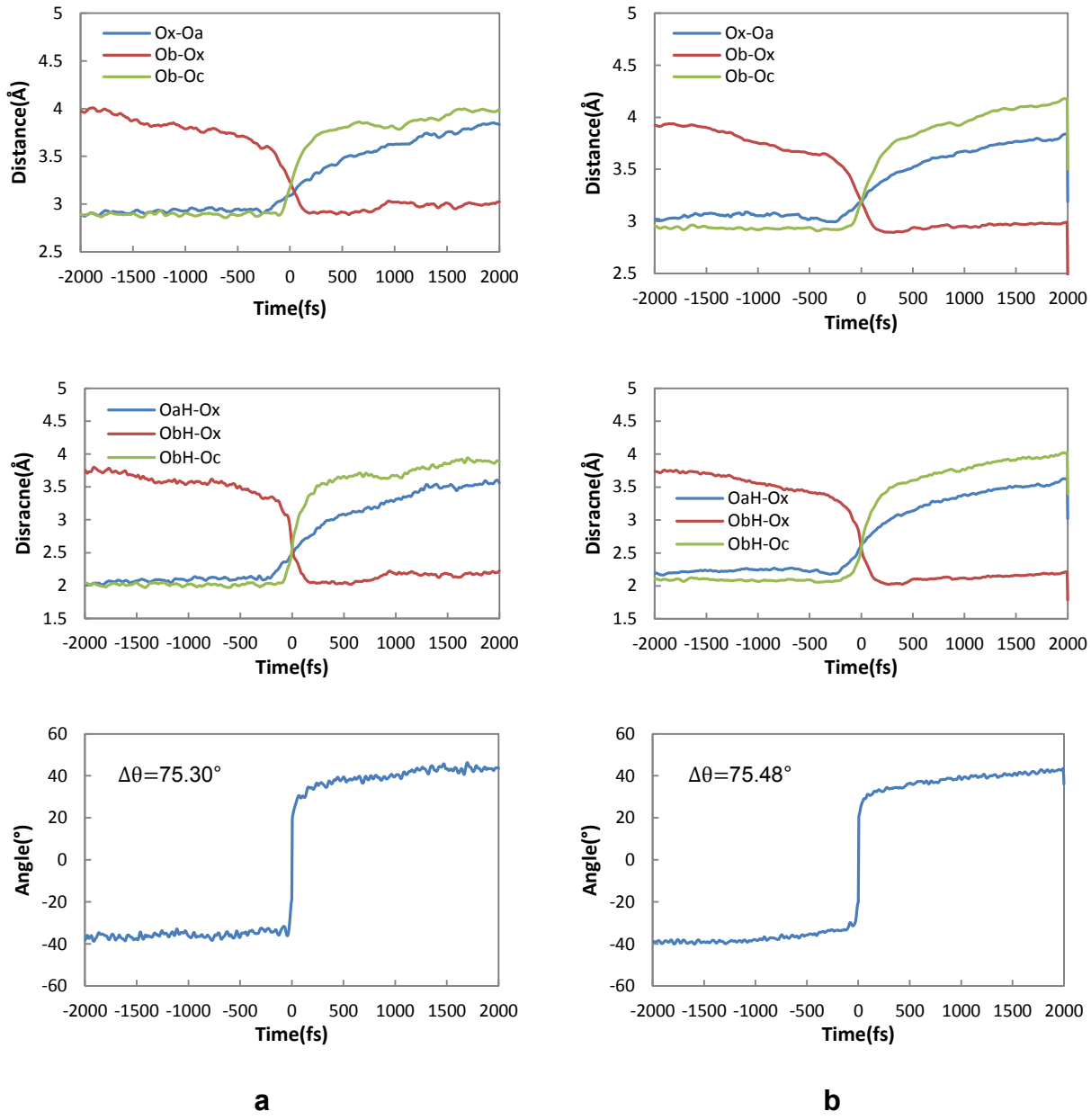

Figure 4.6: Time evolution of the hydrogen bond exchange geometric coordinates for WTH rotations around (a) β-D-glucopyranose and (b) α-D-glucopyranose. The plots are an average of all hydroxyls.

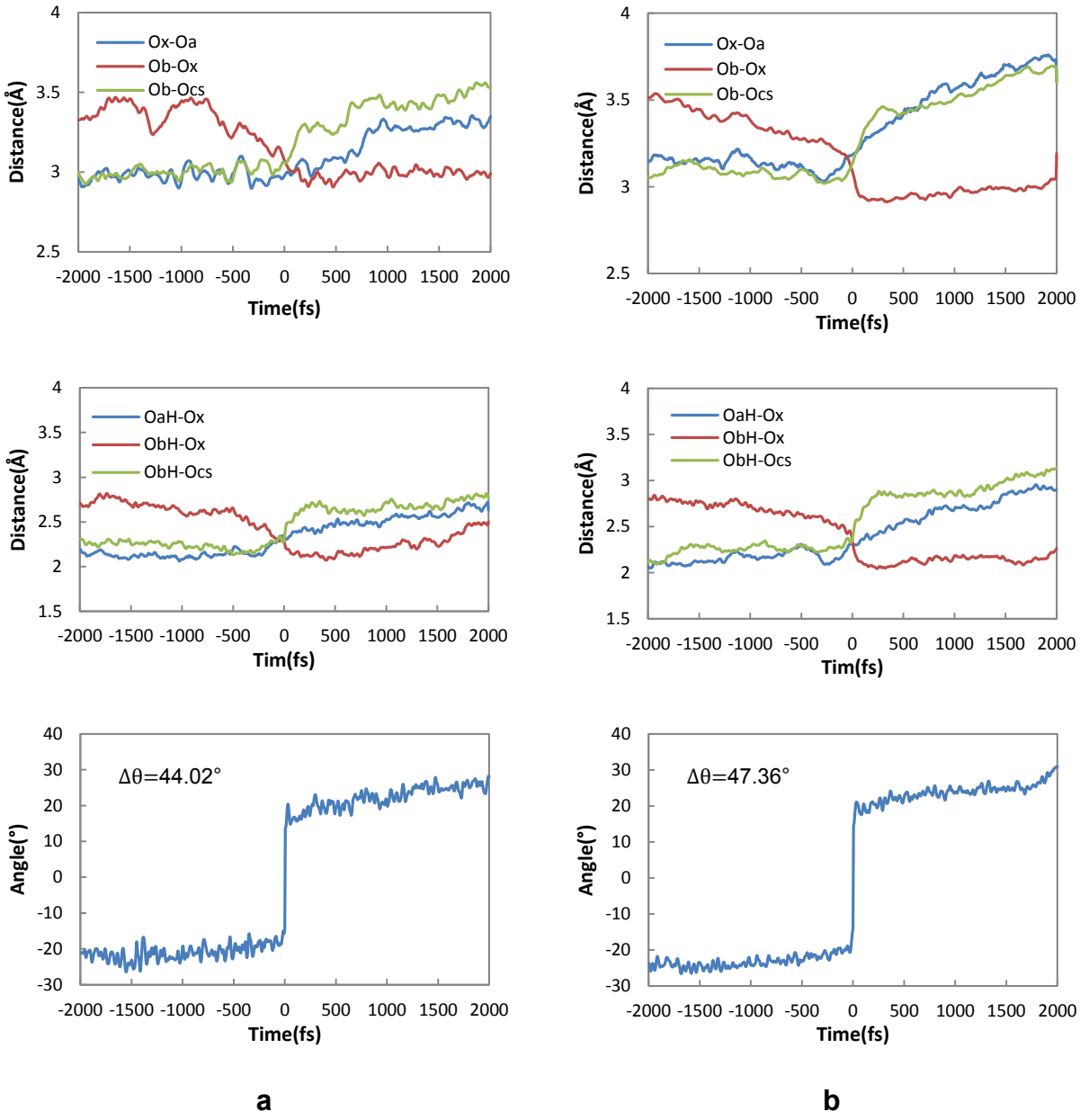

Figure 4.7: Time evolution of the hydrogen bond exchange geometric coordinates for HTH rotations around (a) β-D-glucopyranose and (b) α-D-glucopyranose. The plots are an average of all hydroxyls The plots are an average of all hydroxyls.

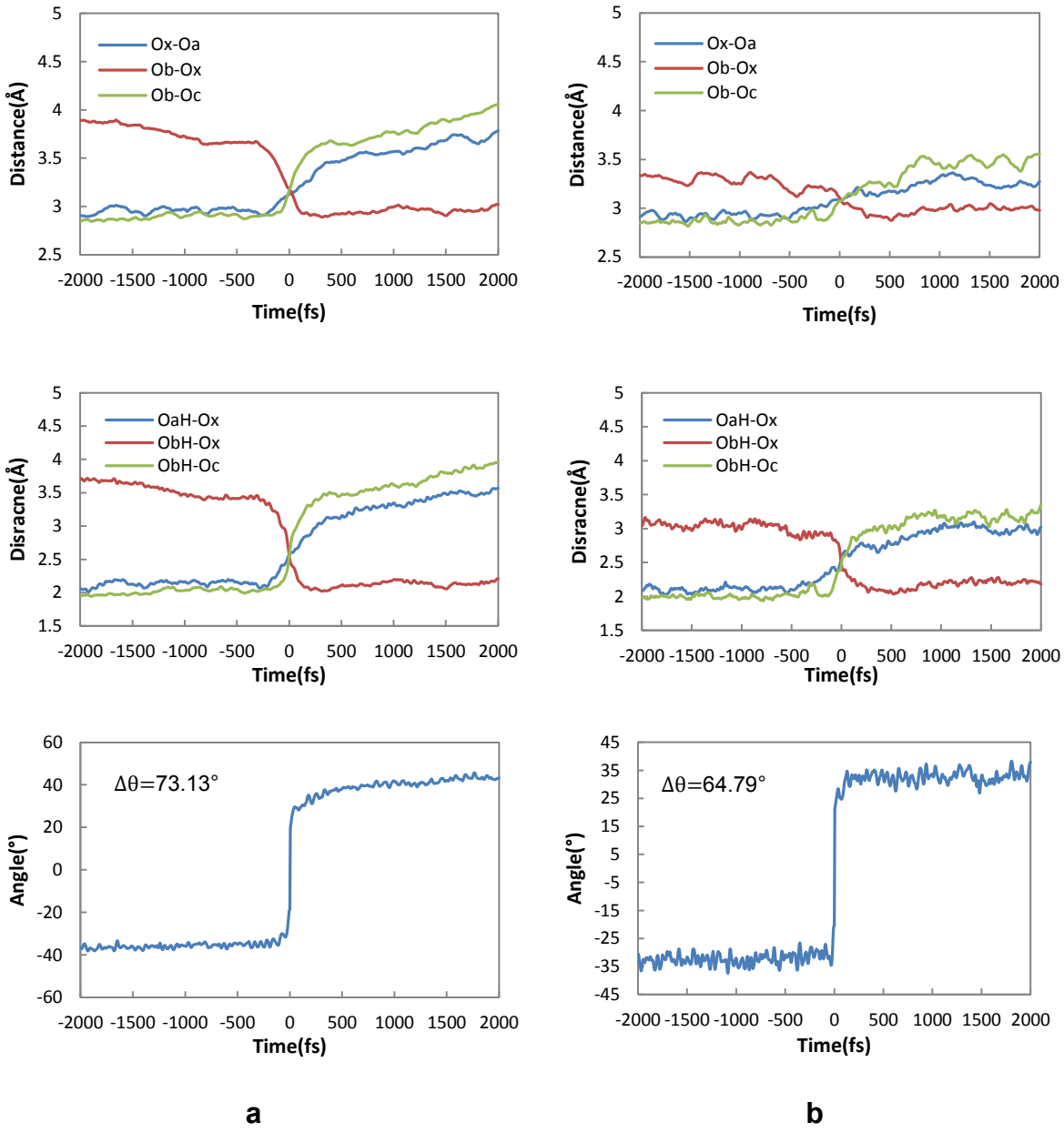

Figure 4.8: Time evolution of the hydrogen bond exchange geometric for WTH rotations around (a) β-D-xyloopyranose and (b) α-D-xylopyranose. The plots are an average of all hydroxyls.

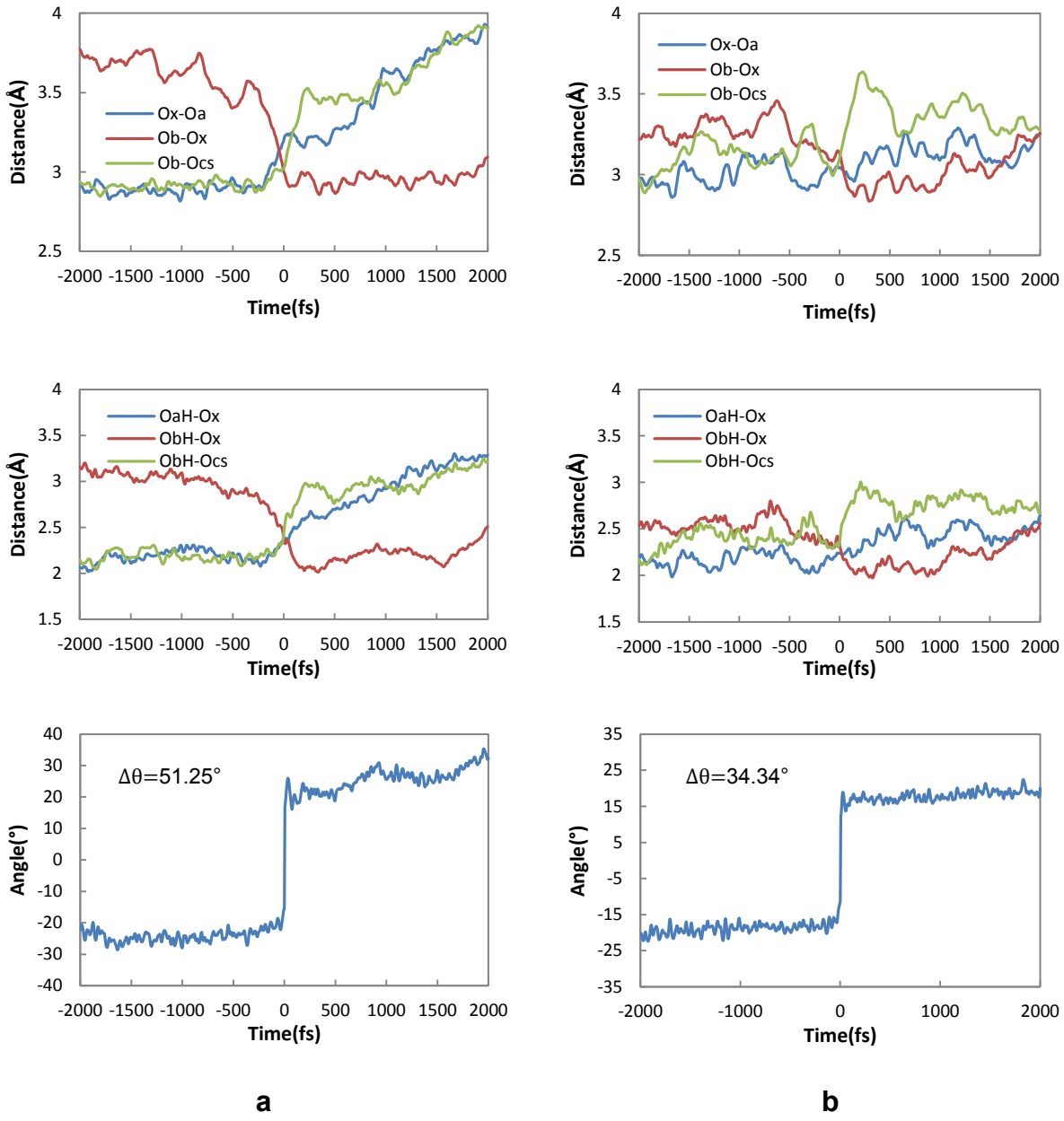

Figure 4.9: Time evolution of the hydrogen bond exchange geometric for HTH rotations around (a) β-D-xyloopyranose and (b) α-D-xylopyranose. The plots are an average of all hydroxyls.

The plots in Figure 4.9 are not well defined. This is in accord with the SDFs (Figure 4.3d). The half moon shapes around α-D-xylopyranose are not well defined as compared to the other sugar molecules. This also suggests that α-D-xylopyranose-water interactions are not as favourable as in the other systems.

From the plots it can be seen that the incoming water molecule starts at a much closer position to O_x in the HTH pathway than in the WTH. This further supports the existence of two rotation pathways. Movement of O_b and O_c closely resembles that of pure water reorientation as discussed in Chapter 3. There is a sharp drop of the $O_x \cdots O_b$ distance near the transition state of the α-D-xylopyranose

The decrease in $O_x \cdots O_b$ distance before the jump and increase in $O_x \cdots O_a$ distance after the jump happens more slowly (≈400 fs) than in pure water (≈250 fs)[69b]. The observed slowdown of water dynamics around hydration shells of the molecules does not correlate with the rotation angles, as no trend is observed for the diffusion rates and the rotation angles. Vila Verde and Kramer made a similar observation in a study on water dynamics around disaccharides.[2e] They showed that the topology of the disaccharide molecules induces a slowdown in the motion of water in their hydration shells. Laage *et al.* showed that the slowdown in water reorientations around hydrophobic groups can be explained by considering the hydrogen bond exchange transition state and taking into account the solute excluded volume.[71] There is steric hindrance induced by the presence of a solute molecule on the incoming (O_b) water molecule and as a result there are less transition state configurations available which results in a slower hydrogen bond exchange rate. This effect is independent of the nature of the solute. It was also shown that the hydrogen bond strength between a water molecule initially donating a hydrogen and an amino acid hydrogen bond acceptor group plays a key role in the formation of the transition state.[84b] Strong hydrogen bond acceptors induce a significant slowdown in water dynamics. The transition state excluded volume effect (TSEV) and the transition state hydrogen bond effect (TSHB) play an important role in water reorientations jump mechanism.

Having established the existence of two water reorientation pathways, the individual pathways were further analysed. For the hydrogen bond exchanges, three conditions were considered:

1. *No Restriction*: When there are no restrictions on the time length of hydrogen bonds either formed or broken. This condition counts all transient hydrogen bond breaking/forming as actual exchanges.
2. *0.5ps Restriction*: When there is a 0.5ps restriction on the time length of hydrogen bonds broken/formed. For this condition, an exchange is said to occur if the hydrogen bond between a water molecule and the hydroxyl group remains broke for longer than 0.5ps, which implies that the new hydrogen bond formed will remain intact longer than 0.5ps. This value is used as it represents the average hydrogen bond lifetime of water as reported in literature.[89]
3. *2.0ps Restriction*: This condition is the same as that in 2 but with a time restriction of 2.0ps for hydrogen bond lifetimes. It has been also been reported that the hydrogen bond lifetime can last longer than 2ps.[90]

Condition 2 and 3 cover the possible range of hydrogen bond lifetimes that have been reported.[89-90] The total number of hydrogen bond exchanges taking place between the water molecule and each sugar molecule is given in Figure 4.10.

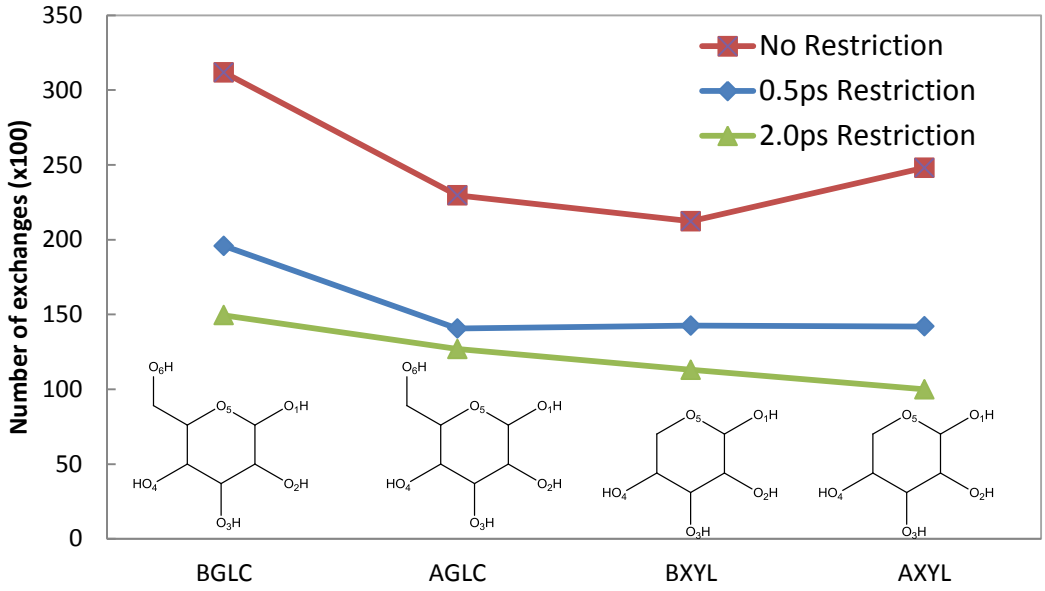

Figure 4.10: Total number of hydrogen bond exchanges taking place around each molecule (WTH & HTH). BGLC= β-D-glucopyranose, AGLC= α-D-glucopyranose, BXYL= β-D-xylopyranose and AXYL = α-D-xylopyranose. Values are calculated from 2ns simulations.

When there are no restrictions, a large number of exchanges take place. This is observed across all systems. Once the 0.5ps Restriction is placed, the number decreases by ~38% across all systems. The 2.0ps Restriction further reduces the number of exchanges observed however the number decreases by ~25%. This indicates that a larger number of water molecules form hydrogen bonds with lifetimes greater than 0.5ps. From the 2.0ps restriction, a trend emerges. The β-anomers have more exchanges taking place than their respective α-anomers. It can also be seen that glucopyranose has more exchanges than xylopyranose.

These hydrogen bond exchanges can be decoupled into water-centred and hydroxyl-centred hydrogen bond exchanges and this is shown in Figure 4.11.

a

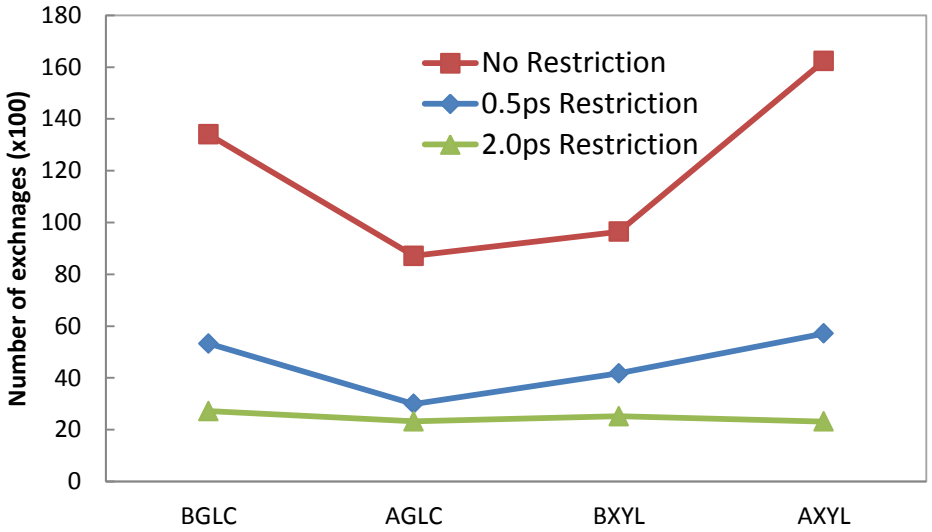

b

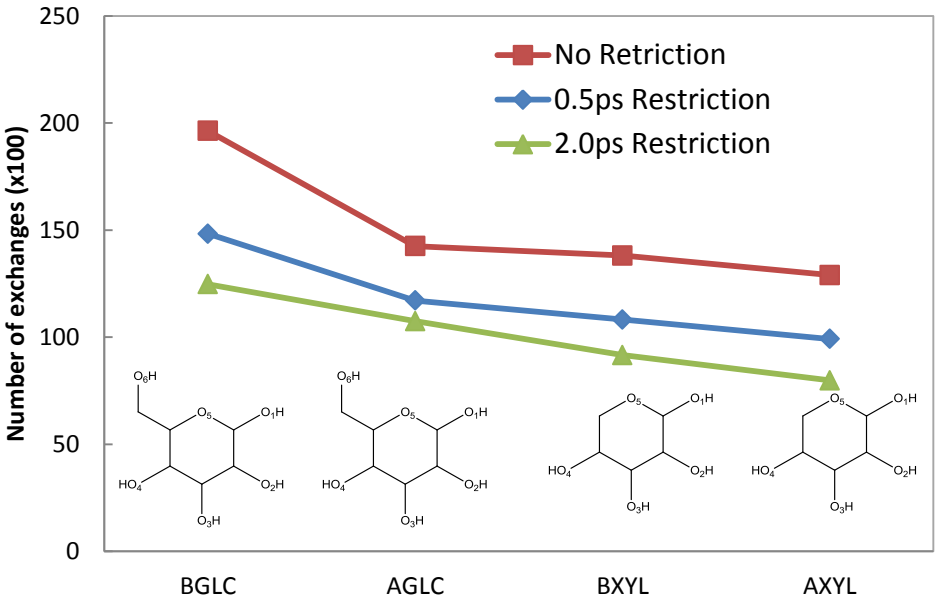

Figure 4.11: Contributions of hydrogen bond exchanges around sugar molecules. (a) Water-centred (b) hydroxyl-centred. BGLC= β-D-glucopyranose, AGLC= α-D-glucopyranose, BXYL= β-D-xylopyranose and AXYL = α-D- xylopyranose.

β-D-glucopyranose maintains a high number of hydrogen bond exchanges in both scenarios of hydrogen bond exchanges, i.e. water-centred and hydroxyl-centred. However, for the water-centred exchanges at the 2.0ps Restriction, the sugar molecules appear to interact with water in the same manner as the number of exchanges is similar across all systems. The 2.0ps Restriction plot in Figure 4.11b shows the same trend as that in Figure 4.10. This indicates that it is the behaviour of

the hydroxyl groups on the sugar molecule that influences the hydration to a larger extent than the water molecules.

The number of WTH hydrogen bond exchanges between water molecules and each hydroxyl group are given in Figure 4.12. The number of exchanges at the 2.0ps Restriction for β-anomers of glucopyranose and xylopyranose are similar. Hydrogen bond exchanges around O1 are higher in both β-anomers, indicating that the β-anomers interact more favourably with water. Across all systems, O5 has the least number of exchanges. This is to be expected as O5 is not a hydroxyl group but is an ether in the ring of the molecules and therefore interactions between the oxygen atom and water is different to that of hydroxyl groups on the molecules. The result is consistent with the RDFs (Figure 4.2). In both glucopyranose anomers O6 has the highest number of exchanges. O1 in both α-anomers of glucopyranose and xylopyranose has less exchanges taking place than O2, O3 and O4. From this result the water probability densities around the sugar molecules can be described as follows; between O1 and O5, β-D-glucopyranose has the highest water probability density, followed by β-D-xylopyranose and α-D-glucopyranose with α-D-xyloopyranose having the smallest water probability density. This corresponds to the number of hydrogen bond exchanges taking place around O1 and decreases in the order β-D-glucopyranose>β-D-xylopyranose>α-D-glucopyranose>α-D-xylopyranose. Therefore the frequent hydrogen bond exchanges around O1 in β-D-glucopyranose results in a higher density in the proximity of the hydroxyl group than around the other sugar molecules. β-D-glucopyranose and β-D-xylopyranose have similar number of WTH hydrogen bond exchanges for O2, O3, O4 and O5 while the trend of the glucopyranose and xylopyranose α-anomers is similar.

a

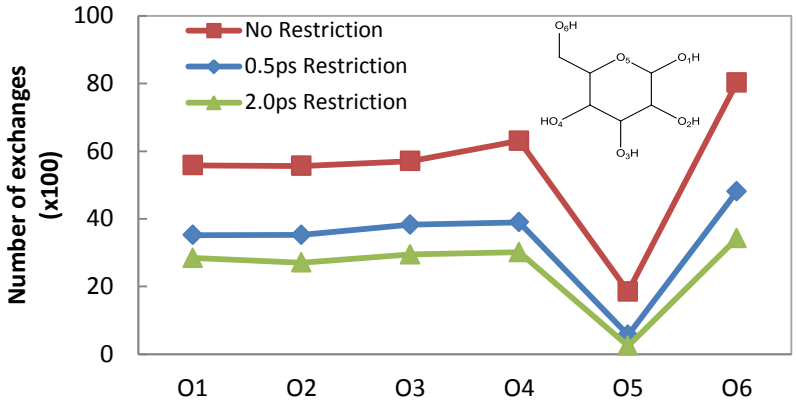

b

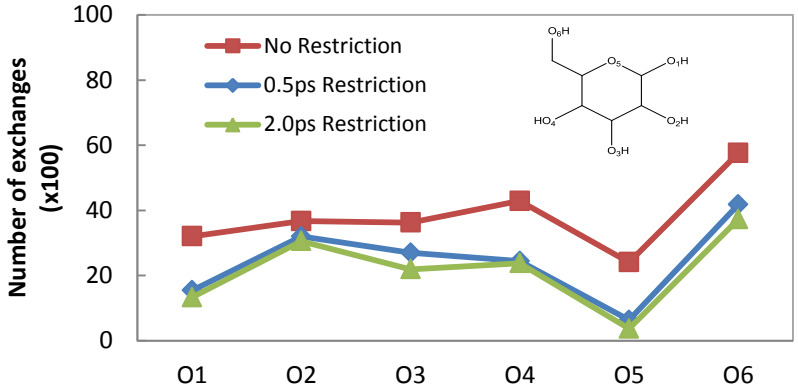

c

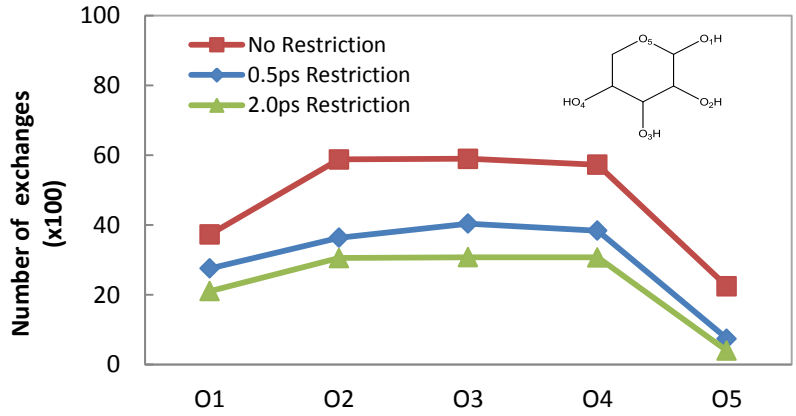

d

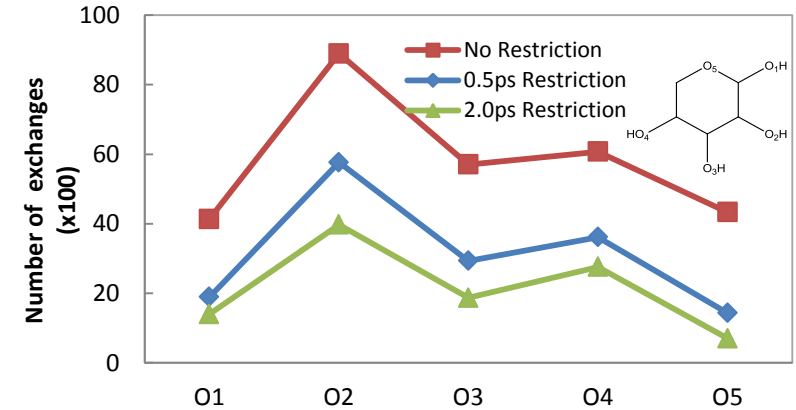

Figure 4.12: Distribution of hydrogen bond exchanges (water-centred + hydroxyl centred) taking place between water molecules and hydroxyl groups of (a) β-D-glucopyranose, (b) α-D-glucopyranose, (c) β-D-xylopyranose and (d) α-D- xylopyranose. O1-O6 represents the respective hydroxyl groups.

To further investigate the origin of the water probability densities, the contributions from water-centred and hydroxyl-centred rotations are separated. Figure 4.13 shows the water-centred hydrogen bond exchanges. The 0.5ps and 2.0ps Restriction plots are similar for β-D-glucopyranose and β-D-xylopyranose. This was also observed with the total number of hydrogen bond exchanges for all sugar molecules (see Figure 4.12). When individual hydroxyl groups are evaluated it can be seen that there are slight differences although the overall behaviour is similar. In β-D-glucopyranose and β-D-xylopyranose there are more exchanges taking place around O4 than around O5. In these two molecules O3 has the highest number of exchanges while in α-D-glucopyranose, O3 has the lowest number of exchanges. The major difference is that noted above with respect to the number of exchanges for O1. Exchanges around the α-anomers show slightly different behaviour when compared to each other.

a

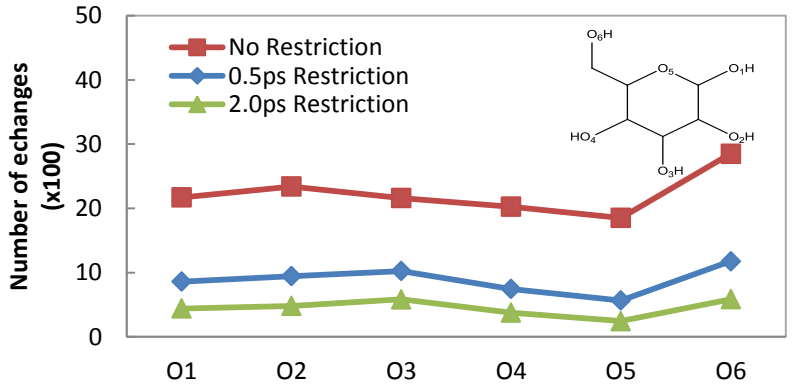

b

c

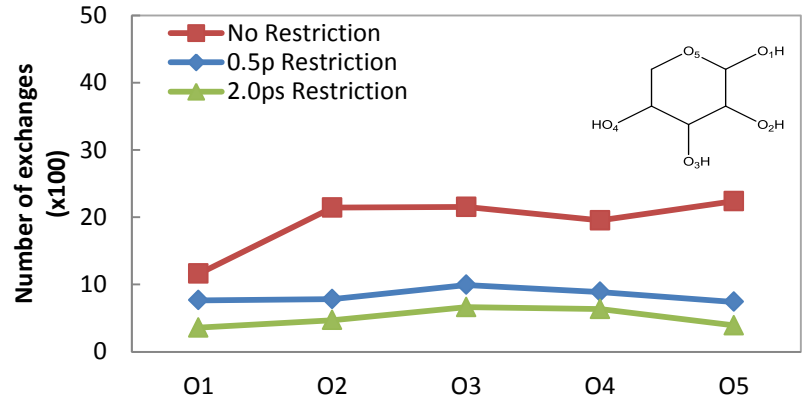

d

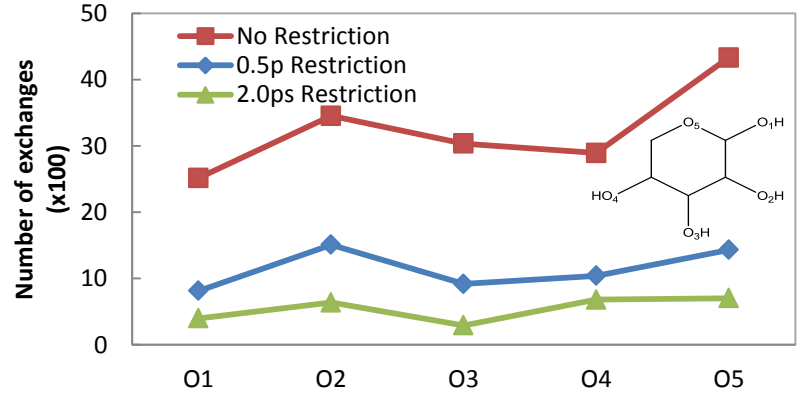

Figure 4.13: Water-centred hydrogen bond exchanges taking place between water molecules and hydroxyl groups of (a) β-D-glucopyranose, (b) (b) α-D-glucopyranose, (c) β-D-xylopyranose and (d) α-D-xylopyranose. O1-O6 represents the respective hydroxyl groups.

a

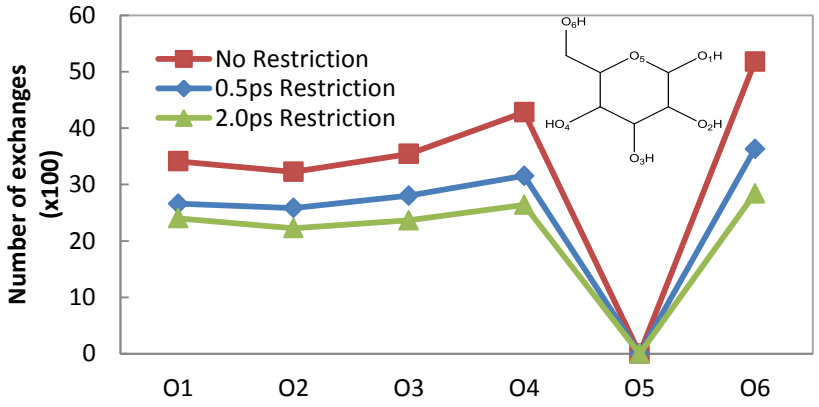

b

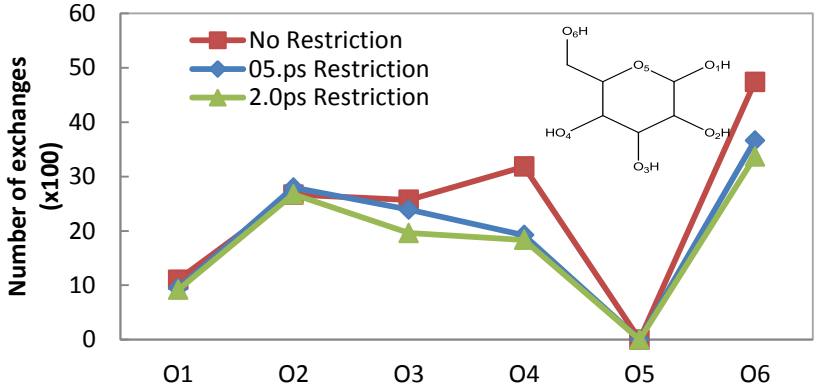

c

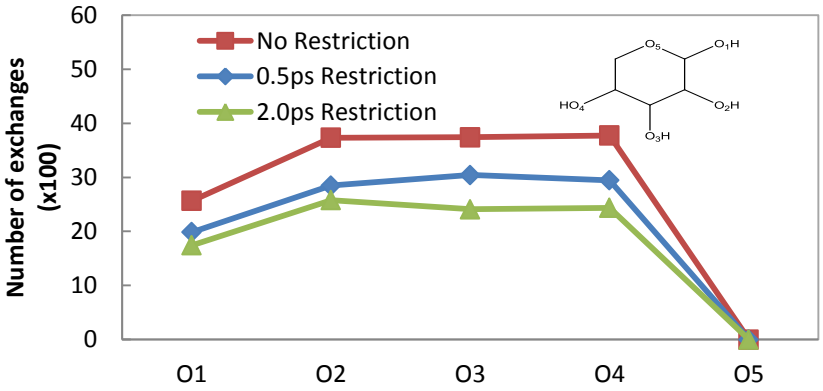

d

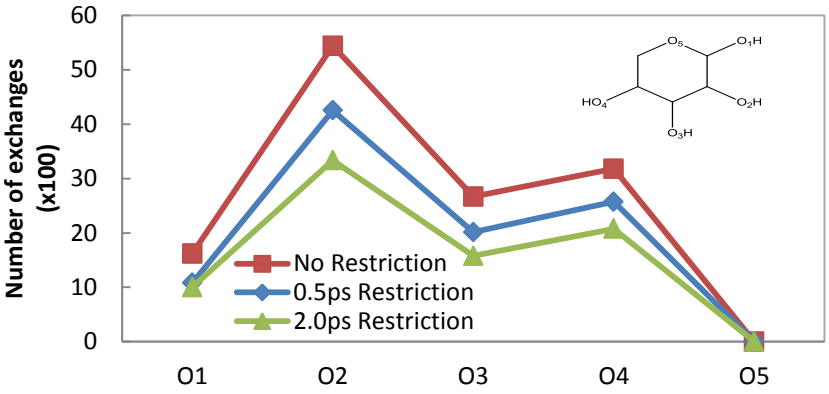

Figure 4.14: Hydroxyl-centred hydrogen bond exchanges taking place between water molecules and hydroxyl groups of (a) β-D-glucopyranose, (b) α-D-glucopyranose, (c) β-D-xylopyranose and (d) α-D-xylopyranose. O1-O6 represents the respective hydroxyl groups.

From Figure 4.14 it can been seen that the hydroxyl-centred exchanges have significant contribution to the overall number of exchanges. This is seen in the similarity of shape of the plots in Figure 4.14 and Figure 4.12.

The final motion of water molecules in the hydration shell of sugar molecules studied is the HTH rotations. The HTH rotation can be described in the following manner: when looking down the plane of the sugar in the $^4C_1$conformation, a water molecule's rotation in the clockwise direction to the adjacent hydroxyl, is said to rotate *from the right* side of the hydroxyl and a counter-clockwise motion is equivalent to rotation *from the left*. An illustration of the rotations is given in Figure 4.15.

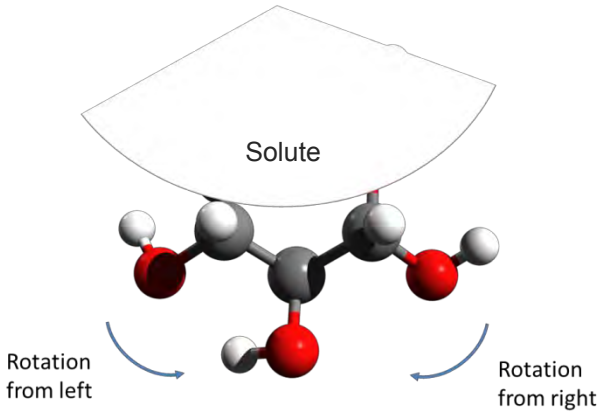

Figure 4.15: Direction of water HTH rotations around neighbouring hydroxyl groups.

The total number of HTH exchanges (Figure 4.16) is significantly less than that of WTH exchanges, thus indicating that the sugar-water interactions are dominated by frequent hydrogen bond exchanges between the water molecules and the hydroxyl groups. The change in number of exchanges from No Restriction to 0.5ps appears to be significant for β-D-glucopyranose and β-D-xylopyranose. In the α-anomers, all three conditions give similar number of exchanges except O2 on α-D-xylopyranose.

a

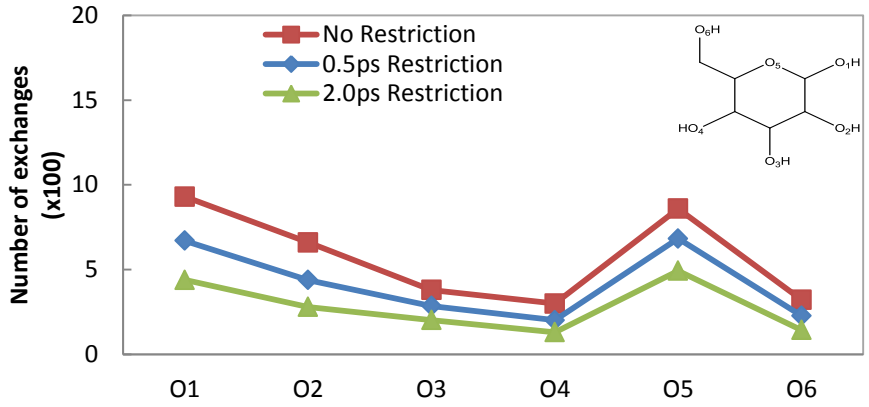

b

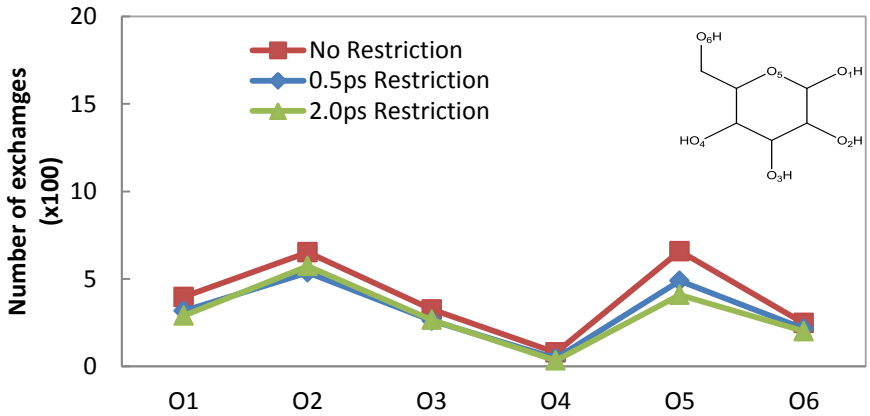

c

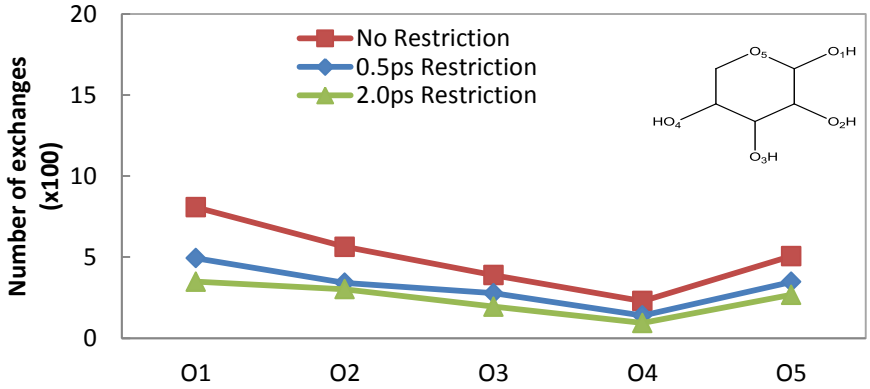

d

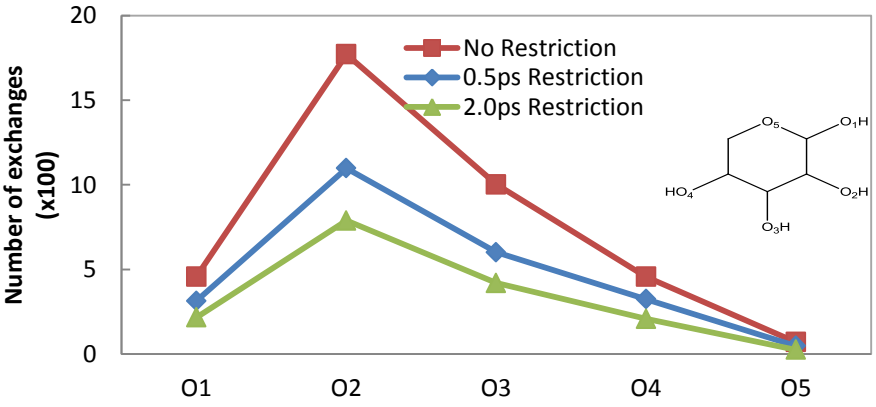

Figure 4.16: HTH hydrogen bond exchanges observed for the sugar molecules, (a) β-D-glucopyranose, (b) α-D-glucopyranose, (c) β-D-xylopyranose and (d) α-D- xylopyranose. O1-O6 represents the respective hydroxyl groups.

For the 2.0ps Restriction, O1 in β-D-glucopyranose has a significantly higher number of HTH exchanges taking place than around α-D-glucopyranose. The plots of the β-anomers from O1 to O5 show the same trend, this is also observed for the α-anomers. For glucopyranose, the β-anomer has more exchanges around O5 while around O6, α-D-glucopyranose has more exchanges.

At the 2.0ps Restriction, O5 of β-D-xylopyranose has a significant number of HTH exchanges while there is almost no HTH exchange activity around α-D-xylopyranose. To understand the origin of this, the HTH exchanges are separated into rotations from the left and from the right as described above. The plots obtained are shown in Figure 4.17 and Figure 4.18.

a

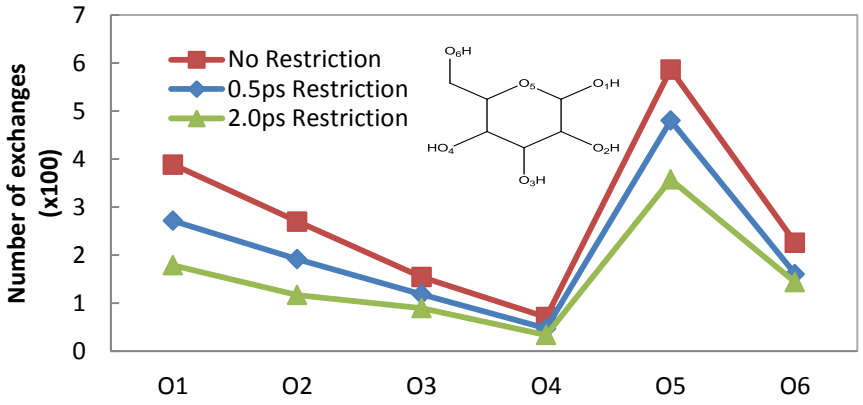

b

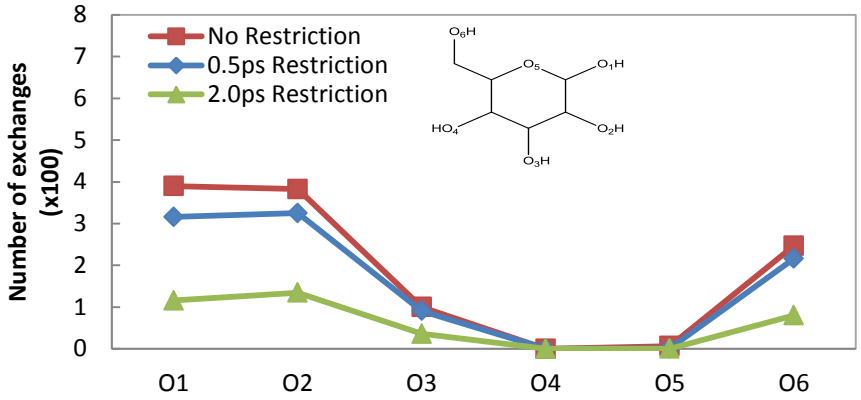

c

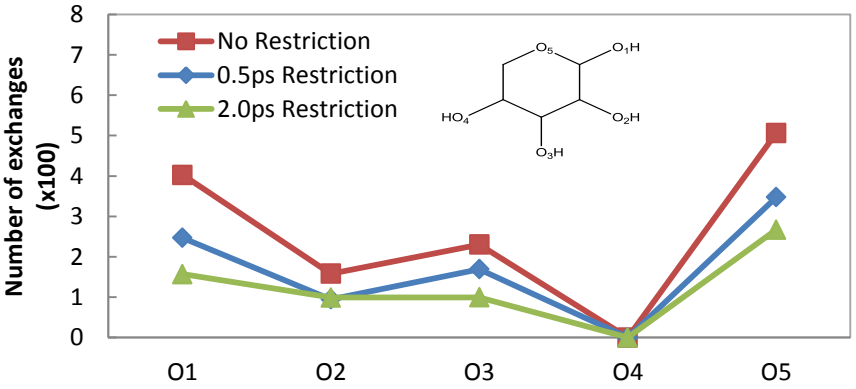

d

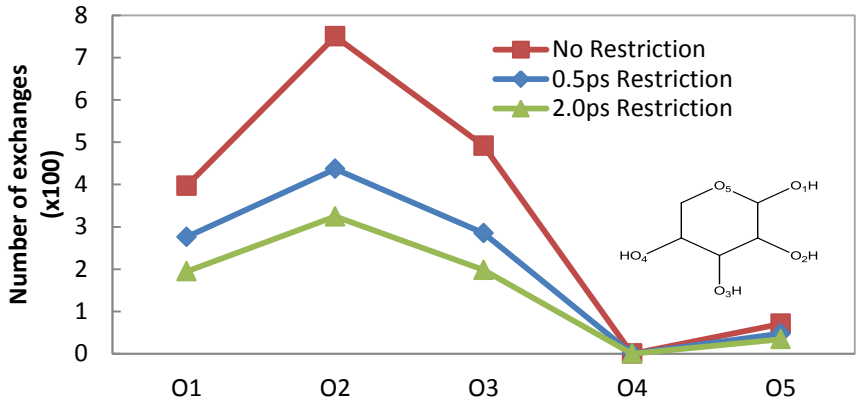

Figure 4.17 Hydrogen bond exchanges around each hydroxyl group for which the HTH exchanges are only from the left of each hydroxyl group. (a) β-D-glucopyranose, (b) α-D-glucopyranose, (c) β-D-xylopyranose and (d) α-D- xylopyranose. O1-O6 represents the respective hydroxyl groups.

a

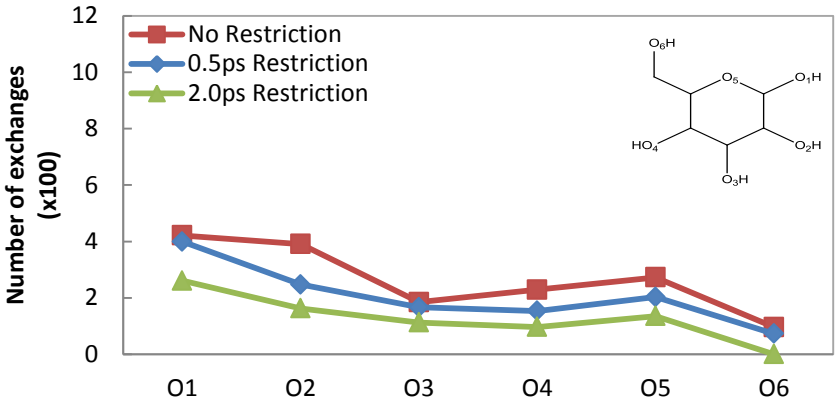

b

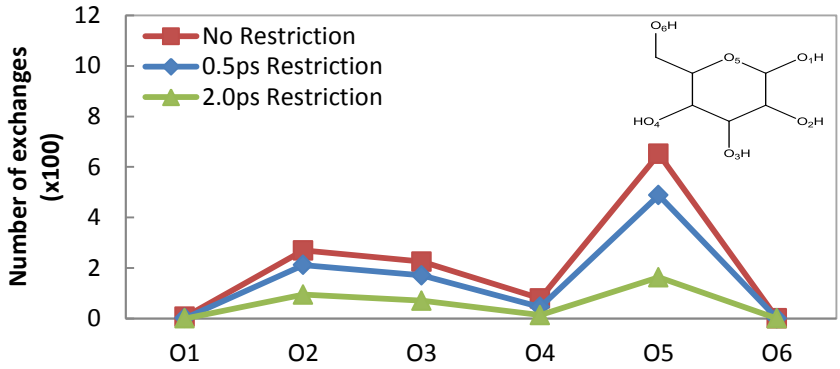

c

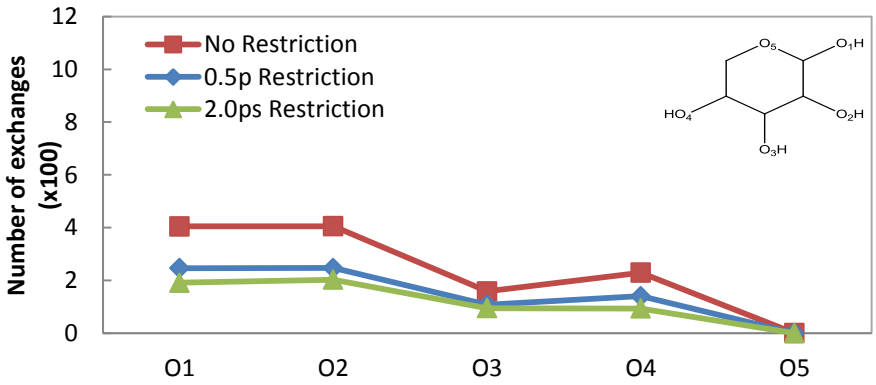

d

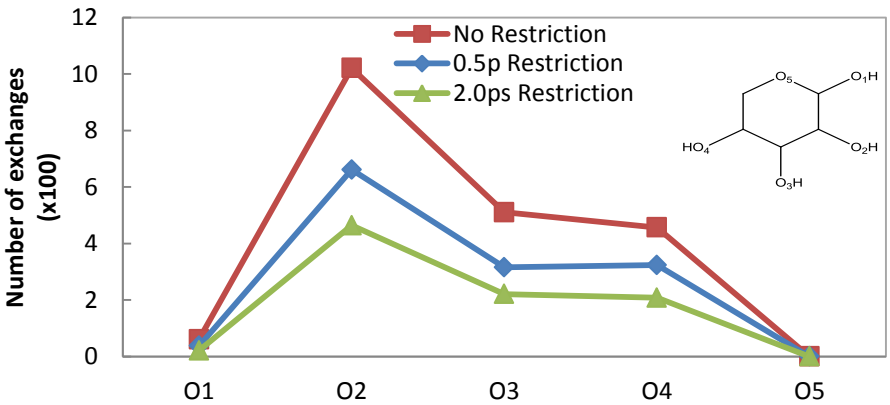

Figure 4.18: Hydrogen bond exchanges around each hydroxyl group for which the HTH exchanges are only from the right of each hydroxyl group. (a) β-D-glucopyranose, (b α-D-glucopyranose, (c) β-D-xylopyranose and (d) α-D- xylopyranose. O1-O6 represents the respective hydroxyl groups.

The α-D-glucopyranose and xylopyranose plots reveal that are no exchanges from the left side of O4 in the two molecules. This is due to the absence of a primary alcohol on xylopyranose and in the case of α-D-glucopyranose, it is a result of the primary alcohol conformation. Hydrogen bond exchanges around O5 on α-D-glucopyranose occur only from the right (O6). This can be attributed to the axial position of the hydroxyl group on the anomeric carbon and also corresponds to a gt conformation of the primary alchohol. These results are consistent with a gt conformation of the primary alcohol being the most favoured conformation as has been previously reported. It was further shown that the preference of this gt conformation is due to the stabilisation provided by the formation of a bridging hydrogen bond between the primary alcohol and the ring oxygen.[2c] A plot of the C4-C5-C6-O6 and O5-C5-C6-O6 dihedral angles (Figure 4.19) shows that it is the gt conformation that is more favoured for glucopyranose. In β-D-glucopyranose the tg and gg conformations are also seen and this accounts for the exchanges observed for O4 coming from the left. The relatively small number of these exchanges indicate that the conformations are less favoured, as has been previously reported.[2c, 91] The primary alcohol conformation can now also be attributed to the hydrogen bond exchange occurring around O1, O5 and O6.

a

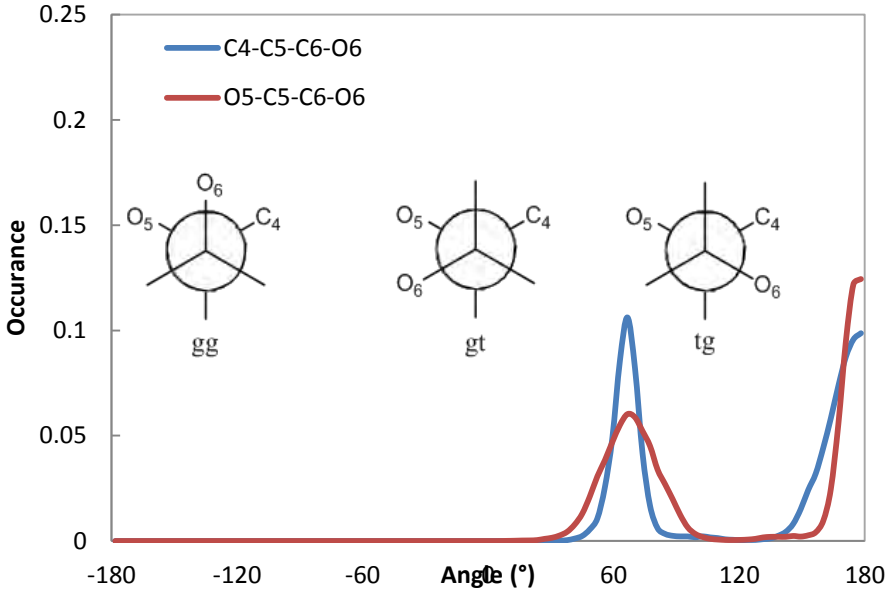

b

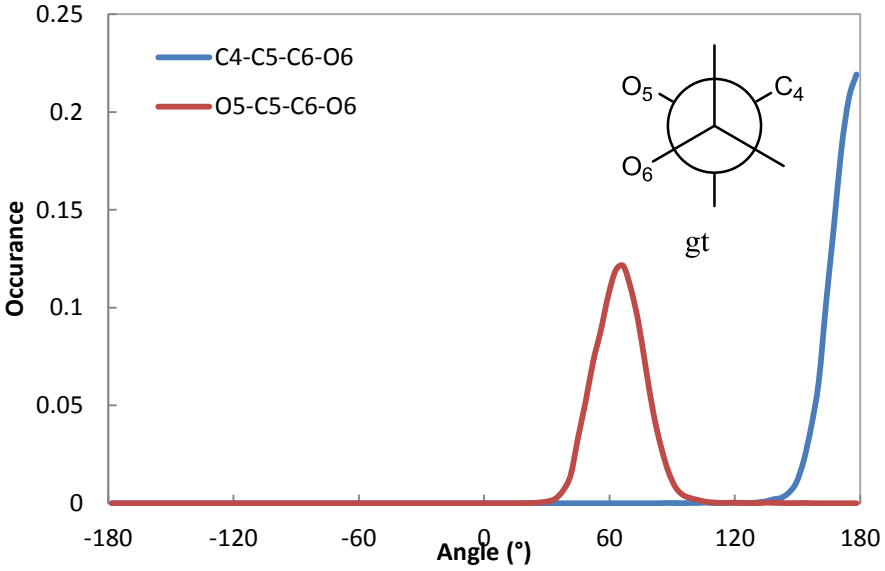

Figure 4.19: Profiles of the primary alcohol dihedral angle orientations (a) β-D-glucopyranose and (b) α-D-glucopyranose. The area under each curve sums up to one. The gt conformation was used as the starting configuration in simulations of both the β-D-glucopyranose and α-D-glucopyranose simulations.

O1, O5 and O6 in β-D-glucopyranose have a relatively high number of HTH exchanges. Evaluation of the HTH exchanges confirms that the high water probability density around O1, O5 and O6 is due to hydrogen bon exchanges exchanging in the O1-O5-O6 region. As this high water density is not seen in α-D-glucopyranose, this result suggests that β-D-glucopyranose is the favoured anomer in solution due this interaction with water molecules. This high water density is also not observed in xylopyranose due to the absence of the primary alcohol.

The results indicate that the primary alcohol together with the relative position of the hydroxyl on the anomeric carbon have a significant role in the hydration of the monosaccharides.

Conclusion

The hydration of monosaccharides was studied with the objective of understanding the interactions between the hydroxyls and water molecules. It was shown that the monosaccharides perturb the water structure, resulting in water forming a hydration shell around solute due to hydrogen bonding between the hydroxyls and water molecules. The second hydration shell around the molecules is not well defined. The association of the water with the solute causes a slowdown in both the translational and rotational motion of water.

The reorientation mechanism of water was studied and shown to be consistent with the molecular jump mechanism reported by Laage. Water reorientation in the hydration shells of sugar molecules occur via the molecular jump mechanism. The presence or two or more hydroxyls adjacent to each other gives rise to two possible reorientation pathways for water molecules, that is, a water molecule rotating from a water-water hydrogen bond to form a water-hydroxyl hydrogen bond and rotation from a water-hydroxyl hydrogen bond to form a water-hydroxyl hydrogen bond with the adjacent hydroxyl. The average rotation angles are larger than in bulk water for water to hydroxyl rotations while water to hydroxyl rotation angles are smaller than bulk water rotation angles.

It is the hydroxyl-centred hydrogen bond exchanges that dominate the overall interaction between hydroxyls and water molecules. This suggests that the hydration of monosaccharides is determined by the intrinsic properties of the individual molecules rather than the solvent molecules.

It was further shown that the presence of a primary alcohol in monosaccharides molecules induces a configuration that allows favourable interactions between water

molecules and hydroxyl groups on the sugar molecules. A region of high water density is formed between the primary alcohol, ring oxygen and the hydroxyl on the anomeric carbon in β-D-glucopyranose. It is not only the presence of the primary alcohol that plays a role in the hydration of the monosaccharides. The relative position of the hydroxyl on the anomeric carbon is shown to create a topology conducive of hydroxyl to hydroxyl hydrogen bond exchanges.

Overall, glucopyranose has more hydroxyl to hydroxyl exchanges than xylopyranose and this corresponds to the solubility of the two sugar molecules. The β-anomers have more favourable interactions with water molecules than with the corresponding α-anomers. This also corresponds with the anomeric ratios of glucopyranose and xylopyranose in solution.

The hydration of monosaccharides has been described in terms of the hydrogen bond exchanges taking place in the solvation shells of the sugar molecules.

References

[1] a) B. R. Brooks, R. E. Bruccoleri, B. D. Olafson, D. J. States, S. Swaminathan and M. Karplus, *J. Comput. Chem.* **1983**, *4*, 187-217; b) W. D. Cornell, P. Cieplak, C. I. Bayly, I. R. Gould, K. M. Merz, D. M. Ferguson, D. C. Spellmeyer, T. Fox, J. W. Caldwell and P. A. Kollman, *JACS* **1995**, *117*, 5179-5197; c) W. L. Jorgensen and J. Tirado-Rives, *JACS* **1988**, *110*, 1657-1666; d) A. Varki, *Glycobiology* **1993**, *3*, 97-130.

[2] a) J. W. Brady, *JACS* **1989**, *111*, 5155-5165; b) M. Kuttel, J. W. Brady and K. J. Naidoo, *J. Comput. Chem.* **2002**, *23*, 1236-1243; c) C. B. Barnett and K. J. Naidoo, *J. Phys. Chem. B* **2008**, *112*, 15450-15459; d) A. Vishnyakov, A. Laaksonen and G. Widmalm, *J. Mol. Graphics Modell.* **2001**, *19*, 338-342; e) A. Vila Verde and R. K. Campen, *J. Phys. Chem. B* **2011**, *115*, 7069-7084; f) E. J. Hehre, *Carbohydr. Res.* **2001**, *331*, 347-368; g) J. Yu-Jen Chen and K. J. Naidoo, *J. Phys. Chem. B* **2003**, *107*, 9558-9566; h) D. Fabri, M. A. K. Williams and T. K. Halstead, *Carbohydr. Res.* **2005**, *340*, 889-905; i) D. Steinborn and H. Junicke, *Chem. Rev.* **2000**, *100*, 4283-4318; j) Y. Mikata, Y. Shinohara, K. Yoneda, Y. Nakamura, I. Brudziñska, T. Tanase, T. Kitayama, R. Takagi, T. Okamoto, I. Kinoshita, M. Doe, C. Orvig and S. Yano, *Biorg. Med. Chem. Lett.* **2001**, *11*, 3045-3047; k) A. V. Demchenko, *Synlett* **2003**, *2003*, 1225,1240; l) C. Vetter, P. Pornsuriyasak, J. Schmidt, N. P. Rath, T. Ruffer, A. V. Demchenko and D. Steinborn, *Dalton Transactions* **2010**, *39*, 6327-6338; m) L. K. Mydock and A. V. Demchenko, *Org. Bio. Chem.* **2010**, *8*, 497-510; n) F. A. Momany, M. Appell, J. L. Willett and W. B. Bosma, *Carbohydr. Res.* **2005**, *340*, 1638-1655; o) P. Pornsuriyasak, C. Vetter, S. Kaeothip, M. Kovermann, J. Balbach, D. Steinborn and A. V. Demchenko, *Chem. Commun.* **2009**, 6379-6381; p) Q. Liu and J. W. Brady, *JACS* **1996**, *118*, 12276-12286.

[3] J. M. Berg, J. L. Tymoczko and L. Stryer, *Biochemistry*, W. H. Freeman \& Co., **1995**, p.

[4] a) S. J. Angyal, *Angewandte Chemie International Edition in English* **1969**, *8*, 157-166; b) G. Lelong, M.-L. Saboungi and J. W. Brady, *Mol. Simulat.* **2012**, *38*, 1186-1197.

[5] A. Kirby in *Stereoelectronic Effects on Reactivity: The Kinetic Anomeric Effect*, *Vol. 15* Springer Berlin Heidelberg, **1983**, pp. 78-135.

[6] M. A. Kabayama and D. Patterson, *Can. J. Chem.* **1958**, *36*, 563-573.

[7] C. J. Cramer and D. G. Truhlar, *JACS* **1993**, *115*, 5745-5753.

[8] W. N. Haworth, *The Constitution of Sugars*, Longmans, Green & Company, **1929**, p.

[9] J. F. Stoddart, *Stereochemistry of carbohydrates*, Wiley-Interscience, New York, **1971**, p.

[10] M. Paolantoni, P. Sassi, A. Morresi and S. Santini, *J. Chem. Phys.* **2007**, *127*, 024504.

[11] D. Laage, G. Stirnemann and J. Hynes, *SCIENCE CHINA Physics, Mechanics & Astronomy* **2010**, *53*, 1068-1072.

[12] U. Talon, L. J. Smith, J. W. Brady, B. A. Lewis, J. R. D. Copley, D. L. Price and M. L. Saboungi, *J. Phys. Chem. B* **2004**, *108*, 5120-5126.

[13] U. Heugen, G. Schwaab, E. Bründermann, M. Heyden, X. Yu, D. M. Leitner and M. Havenith, *PNAS* **2006**, *103*, 12301-12306.

[14] R. Giangiacomo, *Food Chem.* **2006**, *96*, 371-379.

[15] J. Hine and P. K. Mookerjee, *J. Org. Chem.* **1975**, *40*, 292-298.

[16] A. Boscaino and K. J. Naidoo, *J. Phys. Chem. B* **2011**, *115*, 2608-2616.

[17] B. Leroux, H. Bizot, J. W. Brady and V. Tran, *Chem. Phys.* **1997**, *216*, 349-363.
[18] W. Cun Xin, C. Wei Zu, V. Tran and R. Douillard, *Chem. Phys. Lett.* **1996**, *251*, 268-274.
[19] G. Bonanno, R. Noto and S. L. Fornili, *J. Chem. Soc., Faraday Trans.* **1998**, *94*, 2755-2762.
[20] a) D. Russo, G. Hura and T. Head-Gordon, *Biophys. J.* **2004**, *86*, 1852-1862; b) A. R. Bizzarri and S. Cannistraro, *J. Phys. Chem. B* **2002**, *106*, 6617-6633; c) M. Marchi, F. Sterpone and M. Ceccarelli, *JACS* **2002**, *124*, 6787-6791.
[21] F. H. Stillinger, *Science* **1980**, *209*, 451-457.
[22] D. Eisenberg and W. Kauzmann, *The Structure and Properties of Water*, Oxford University Press, Oxford, **2005**, p.
[23] L. Verlet, *Phys. Rev.* **1967**, *159*, 98-103.
[24] a) N. L. Allinger, *JACS* **1977**, *99*, 8127-8134; b) B. J. Alder and T. E. Wainwright, *J. Chem. Phys.* **1960**, *33*, 1439-1451; c) R. W. Hockney and J. W. Eastwood, *Computer simulation using particles*, Taylor & Francis, Inc., **1988**, p. 564.
[25] S. B. Engelsen, C. Monteiro, C. Hervé De Penhoat and S. Pérez, *Biophys. Chem.* **2001**, *93*, 103-127.
[26] K. J. Naidoo and J. Y. J. Chen, *Mol. Phys.* **2003**, *101*, 2687-2694.
[27] L. Lupi, L. Comez, M. Paolantoni, S. Perticaroli, P. Sassi, A. Morresi, B. M. Ladanyi and D. Fioretto, *J. Phys. Chem. B* **2012**, *116*, 14760-14767.
[28] M. E. Gallina, P. Sassi, M. Paolantoni, A. Morresi and R. S. Cataliotti, *J. Phys. Chem. B* **2006**, *110*, 8856-8864.
[29] L. R. Winther, J. Qvist and B. Halle, *J. Phys. Chem. B* **2012**, *116*, 9196-9207.
[30] S. Perticaroli, M. Nakanishi, E. Pashkovski and A. P. Sokolov, *J. Phys. Chem. B* **2013**, *117*, 7729-7736.
[31] H. Yuasa and H. Hashimoto, *JACS* **1999**, *121*, 5089-5090.
[32] T. Mizuochi and A. Kobata, *Biochem. Biophys. Res. Commun.* **1980**, *97*, 772-778.
[33] W. I. Weis, K. Drickamer and W. A. Hendrickson, *Nature* **1992**, *360*, 127-134.
[34] Y.-J. Zheng, R. L. Ornstein and J. A. Leary, *J. Mol. Struc. THEOCHEM* **1997**, *389*, 233-240.
[35] D. Laage and J. T. Hynes, *Science* **2006**, *311*, 832-835.
[36] A. Leach, *Molecular Modelling: Principles and Applications (2nd Edition)*, Prentice Hall, **2001**, p.
[37] E. Lewars, *Computational Chemistry: Introduction to the Theory and Applications of Molecular and Quantum Mechanics*, Kluwer Academic Publishers, **2004**, p.
[38] A. D. Mackerell, *J. Comput. Chem.* **2004**, *25*, 1584-1604.
[39] N. L. Allinger in *Calculation of Molecular Structure and Energy by Force-Field Methods*, *Vol. Volume 13* Eds.: V. Gold and D. Bethell), Academic Press, **1976**, pp. 1-82.
[40] A. D. MacKerell, N. Banavali and N. Foloppe, *Biopolymers* **2000**, *56*, 257-265.
[41] W. L. Jorgensen, D. S. Maxwell and J. Tirado-Rives, *JACS* **1996**, *118*, 11225-11236.
[42] A. K. Soper, *Chem. Phys.* **2000**, *258*, 121-137.
[43] A. D. MacKerell, D. Bashford, Bellott, R. L. Dunbrack, J. D. Evanseck, M. J. Field, S. Fischer, J. Gao, H. Guo, S. Ha, D. Joseph-McCarthy, L. Kuchnir, K. Kuczera, F. T. K. Lau, C. Mattos, S. Michnick, T. Ngo, D. T. Nguyen, B. Prodhom, W. E. Reiher, B. Roux, M. Schlenkrich, J. C. Smith, R. Stote, J. Straub, M. Watanabe, J.

Wiórkiewicz-Kuczera, D. Yin and M. Karplus, *J. Phys. Chem. B* **1998**, *102*, 3586-3616.
[44] a) N. L. Allinger, M. T. Tribble, M. A. Miller and D. H. Wertz, *JACS* **1971**, *93*, 1637-1648; b) O. Guvench, E. Hatcher, R. M. Venable, R. W. Pastor and A. D. MacKerell, *J. Chem. Theo. Comp.* **2009**, *5*, 2353-2370; c) K. Vanommeslaeghe, E. Hatcher, C. Acharya, S. Kundu, S. Zhong, J. Shim, E. Darian, O. Guvench, P. Lopes, I. Vorobyov and A. D. Mackerell, *J. Comput. Chem.* **2010**, *31*, 671-690.
[45] W. L. Jorgensen, J. Chandrasekhar, J. D. Madura, R. W. Impey and M. L. Klein, *J. Chem. Phys.* **1983**, *79*, 926-935.
[46] H. J. C. Berendsen, J. R. Grigera and T. P. Straatsma, *J. Phys. Chem.* **1987**, *91*, 6269-6271.
[47] H. W. Horn, W. C. Swope, J. W. Pitera, J. D. Madura, T. J. Dick, G. L. Hura and T. Head-Gordon, *J. Chem. Phys.* **2004**, *120*, 9665-9678.
[48] M. W. Mahoney and W. L. Jorgensen, *J. Chem. Phys.* **2000**, *112*, 8910-8922.
[49] A. Godec and F. Merzel, *JACS* **2012**, *134*, 17574-17581.
[50] K. R. Wilson, B. S. Rude, T. Catalano, R. D. Schaller, J. G. Tobin, D. T. Co and R. J. Saykally, *J. Phys. Chem. B* **2001**, *105*, 3346-3349.
[51] L. V. Hooper, S. M. Manzella and J. U. Baenziger, *The FASEB Journal* **1996**, *10*, 1137-1146.
[52] L. S. Bartell, *JACS* **1977**, *99*, 3279-3282.
[53] K. N. Kirschner, A. B. Yongye, S. M. Tschampel, J. González-Outeiriño, C. R. Daniels, B. L. Foley and R. J. Woods, *J. Comput. Chem.* **2008**, *29*, 622-655.
[54] a) R. Kumar, J. R. Schmidt and J. L. Skinner, *J. Chem. Phys.* **2007**, *126*, 204107-204112; b) A. H. Narten and H. A. Levy, *J. Chem. Phys.* **1971**, *55*, 2263-2269; c) G. Hura, J. M. Sorenson, R. M. Glaeser and T. Head-Gordon, *J. Chem. Phys.* **2000**, *113*, 9140-9148.
[55] M. P. Allen and D. J. Tildesley, *Computer Simulation of Liquids*, Clarendon Press, Oxford, **1987**, p.
[56] P. J. Steinbach and B. R. Brooks, *J. Comput. Chem.* **1994**, *15*, 667-683.
[57] a) L. Onsager, *JACS* **1936**, *58*, 1486-1493; b) P. A. Wood, F. H. Allen and E. Pidcock, *CrystEngComm* **2009**, *11*, 1563-1571.
[58] G. Kansas, *Blood* **1996**, *88*, 3259-3287.
[59] T. Darden, D. York and L. Pedersen, *J. Chem. Phys.* **1993**, *98*, 10089-10092.
[60] P. Murray-Rust and J. P. Glusker, *JACS* **1984**, *106*, 1018-1025.
[61] A. Szabo and N. Ostlund, *Modern Quantum Chemistry: Introduction to Advanced Electronic Structure Theory (Dover Books on Chemistry)*, Dover Publications, **1996**, p.
[62] a) K. A. Jebber, K. Zhang, C. J. Cassady and A. Chung-Phillips, *JACS* **1996**, *118*, 10515-10524; b) C. Molteni and M. Parrinello, *JACS* **1998**, *120*, 2168-2171.
[63] P. B. Balbuena and J. M. Seminario, *Molecular Dynamics: From Classical to Quantum Methods*, Elsevier Science & Technology Books, **1999**, p.
[64] H. Granicher, C. Jaccard, P. Scherrer and A. Steinemann, *Discussions of the Faraday Society* **1957**, *23*, 50-62.
[65] R. F. W. Bader, *Atoms in molecules : a quantum theory*, Clarendon Press, Oxford; New York, **1990**, p.
[66] D. A. Pearlman, D. A. Case, J. W. Caldwell, W. S. Ross, T. E. Cheatham Iii, S. DeBolt, D. Ferguson, G. Seibel and P. Kollman, *Comput. Phys. Commun.* **1995**, *91*, 1-41.
[67] R. Podeszwa and V. Buch, *Phys. Rev. Lett.* **1999**, *83*, 4570.

[68] a) G. J. Martyna, M. E. Tuckerman, D. J. Tobias and M. L. Klein, *Mol. Phys.* **1996**, *87*, 1117-1157; b) M. Prall, *J. Comput. Chem.* **2001**, *22*, 132-134.
[69] a) D. Laage and J. T. Hynes, *J. Phys. Chem. B* **2008**, *112*, 14230-14242; b) D. Laage, *Science* **2006**, *311*, 832-835.
[70] a) G. Stirnemann, P. J. Rossky, J. T. Hynes and D. Laage, *Faraday Discuss.* **2010**, *146*, 263-281; b) G. Stirnemann and D. Laage, *J. Phy. Chem. Lett.* **2010**, *1*, 2046-2046.
[71] D. Laage, G. Stirnemann and J. T. Hynes, *J. Phys. Chem. B* **2009**, *113*, 2428-2435.
[72] Y. L. A. Rezus and H. J. Bakker, *Phys. Rev. Lett.* **2007**, *99*, 148301.
[73] D. Laage and J. T. Hynes, *PNAS* **2007**, *104*, 11167-11172.
[74] J.-P. Ryckaert, G. Ciccotti and H. J. C. Berendsen, *J. Comput. Phys.* **1977**, *23*, 327-341.
[75] I.-C. Yeh and G. Hummer, *J. Phys. Chem. B* **2004**, *108*, 15873-15879.
[76] a) R. Mills, *J. Phys. Chem.* **1973**, *77*, 685-688; b) W. S. Price, H. Ide and Y. Arata, *J. Phys. Chem. A* **1999**, *103*, 448-450; c) H. Y. Carr and E. M. Purcell, *Phys. Rev.* **1954**, *94*, 630.
[77] a) I. M. Svishchev and P. G. Kusalik, *J. Chem. Phys.* **1993**, *99*, 3049-3058; b) I. Ohmine and H. Tanaka, *Chem. Rev.* **1993**, *93*, 2545-2566.
[78] D. Laage and J. T. Hynes, *J. Phys. Chem. B* **2008**, *112*, 7697-7701.
[79] a) W. Drost-Hansen, *Science* **1969**, *166*, 861; b) H. E. Stanley, P. Kumar, L. Xu, Z. Yan, M. G. Mazza, S. V. Buldyrev, S. H. Chen and F. Mallamace, *Physica A: Statistical Mechanics and its Applications* **2007**, *386*, 729-743.
[80] N. Nandi and B. Bagchi, *J. Phys. Chem. B* **1997**, *101*, 10954-10961.
[81] K. J. Tielrooij, S. T. van der Post, J. Hunger, M. Bonn and H. J. Bakker, *J. Phys. Chem. B* **2011**, *115*, 12638-12647.
[82] a) M. D. Fayer, *Acc. Chem. Res.* **2011**, *45*, 3-14; b) J. T. King and K. J. Kubarych, *JACS* **2012**, *134*, 18705-18712.
[83] a) S. L. Lee, P. G. Debenedetti and J. R. Errington, *J. Chem. Phys.* **2005**, *122*, 204511; b) N. Bhattacharjee and P. Biswas, *J. Phys. Chem. B* **2011**, *115*, 12257-12265.
[84] a) D. Laage, G. Stirnemann, F. Sterpone, R. Rey and J. T. Hynes in *Reorientation and Allied Dynamics in Water and Aqueous Solutions*, *Vol. 62* Eds.: S. R. Leone, P. S. Cremer, J. T. Groves and M. A. Johnson), **2011**, pp. 395-416; b) F. Sterpone, G. Stirnemann, J. T. Hynes and D. Laage, *J. Phys. Chem. B* **2010**, *114*, 2083-2089.
[85] C. Sagui and T. A. Darden, *Annu. Rev. Biophys. Biomol. Struct.* **1999**, *28*, 155-179.
[86] J. K. Gladden and M. Dole, *JACS* **1953**, *75*, 3900-3904.
[87] H. Ueadaira and H. Uedaira, *Bull. Chem. Soc. Jpn.* **1969**, *42*, 2140-2142.
[88] a) G. Stirnemann, S. R.-V. Castrillon, J. T. Hynes, P. J. Rossky, P. G. Debenedetti and D. Laage, *Phys. Chem. Chem. Phys.* **2011**, *13*, 19911-19917; b) S. Park, M. Odelius and K. J. Gaffney, *J. Phys. Chem. B* **2009**, *113*, 7825-7835.
[89] a) H. F. M. C. Martiniano and N. Galamba, *J. Phys. Chem. B* **2013**, *117*, 16188-16195; b) R. Lamanna, G. Floridi and S. Cannistraro, *Physical Review E* **1995**, *52*, 4529.
[90] V. Voloshin and Y. Naberukhin, *J. Struct. Chem.* **2009**, *50*, 78-89.
[91] a) E. A. Larsson, J. Ulicny, A. Laaksonen and G. Widmalm, *Org. Lett.* **2002**, *4*, 1831-1834; b) R. Stenutz, I. Carmichael, G. Widmalm and A. S. Serianni, *J. Org.*

Chem. **2002**, *67*, 949-958; c) Y. Nishida, H. Ohrui and H. Meguro, *Tetrahedron Lett.* **1984**, *25*, 1575-1578.